Designing zero-mode waveguides for fluorescence experiments on α-synuclein and DNA

Masters' thesis
Education and Communication in the Beta Sciences

July 2022

Author
F.H.C. (Frank) van Loenhout

Exam committee
G. (Gobert) Heesink
Ing. R. (Robert) Molenaar
Dr. L. (Lantian) Chang
Dr. C. (Christian) Blum
Prof. Dr. M.M.A.E. (Mireille) Claessens

Nanobiophysics Group
Faculty of Science & Technology

UNIVERSITY OF TWENTE.

Abstract

Zero-mode waveguides (ZMW) are a mechanical way to lower the detection volume in fluorescence detection methods like Fluorescence Correlation Spectroscopy (FCS) and Two Colour Coincident Detection (TCCD) experiments. The decrease of detection volume allows for single molecule detection experiments at concentrations up to a thousand times higher than the ones accessible by conventional methods. Apart from restricting the detection volume, these waveguides are also reported to enhance fluorescence signal and quench fluorophore lifetime. These properties make ZMWs promising assets when investigating molecular dynamics or aggregation, for instance in the ongoing research into alpha-synuclein. This thesis will design, fabricate and test ZMW to assess their suitability to probe biomolecular interactions. To that end, the performance of the ZMW in terms of signal enhancement, lifetime quenching and restriction of the observation volume is evaluated. After establishing the functionality, interaction experiments with alpha-synuclein and DNA are performed.

I would like to thank both Robert and Gobert for their amazing help during the past 20 weeks, especially concerning your help in the lab and our discussions. I could not have done this without the two of you.

Additionally, I would like to thank Henk van Wolferen and Melissa Goodwin for fabricating the many waveguides I asked for.

Take Care!

Frank

Contents

Chapter 1

Introduction

Alpha-synuclein (aSyn) [1] is an abundant protein in the brain, specifically in the terminals of nerve cells. It is a smalla nd dynamic molecule: the monomers can adopt into various conformational states. As a result, aSyn has various putative functions in the human body: for instance, it is believed it plays a role in the regulation of dopamine release, regulation of cell viability and the regulation of glucose levels [2], [3].The downside of the conformational freedom of aSyn is its tendency to self-aggregate.The monomers might combine or interact, forming multimers. These multimers are transient - they form and are broken down continuously. However, due to genetic or environmental factors [4], they might accumulate and eventually form stable fibrils which in turn can combine into bigger aggregates in the nerve cells. These abnormal aggregates, called Lewy bodies, form the link between aSyn and various neurodegenerative diseases like Alzheimer's and Parkinson's. After Spillantini et al. [5] discovered the involvement of aSyn in 1997, its role in the creation of these and other diseases has been established. In order to slow down these diseases more about aSyn needs to be learned, where particular interest lies in the mechanisms underlying its assembly and aggregation.

The main way in which insight about aSyn can be gained is the use of (single molecule) fluorescence methods like single molecule FRET and FCS, the basics of which will be explained in the next section. Current techniques face limitations however. The most important challenge is one of fundamental nature: optical microscopy and spectroscopy are limited by the diffraction limit of light which in turn limits the maximum concentrations at which single molecule experiments can be conducted. Another challenge concerns the collection of signal from single molecules: low signal to noise ratio and low event rate cause long data acquisition times. Furthermore, the lifetimes of the fluorophores restrict the accessible time scales at which samples can be measured. These factors make it difficult to investigate for instance dynamics or the mechanisms involved in the aggregation of aSyn.

Zero-mode waveguides (ZMWs) provide a solution to these problems ([6], [7], [8]). By mechanically restricting the detection volume of the microscope the limit on the maximum concentration is increased, allowing for single molecule experiments at higher concentrations. Additionally ZMWs increase radiative rate of fluorophores which increases the signal and they allow for detection of nanosecond dynamics by quenching fluorescence lifetime. The goal of this thesis is to design, fabricate and test ZMWs that can be used to probe biomolecular interactions of aSyn. The remainder of this chapter lays out the ground work required for the concepts described in further chapters. Chapter 2 describes the methods, from the workings of the FCS setup to the data analysis and the passivation protocol. Chapter 3 walks through the design process used to fabricate the prototype ZMWs used in these experiments. It will elaborate on the three most important parameters and describe the fabrication technique used to manufacture the waveguides. It will also show the validation experiments, proving that the ZMWs work as intended. Chapter 4 will describe the experiments of interest, using aSyn and DNA. Finally, chapter 5 will conclude this research and provide an outlook on further possible research directions and remaining points of attention.

1.1 Fluorescence

In order to detect molecules, fluorescence can be used. A detailed explanation of this phenomenon is out of the scope for this thesis, but to aid understanding of the measurement techniques in question, a broad introduction to the topic is in place. The information presented here is based on the book by J. Lakowicz [9], more information can be found there.

Fluorescence is a form of luminescence: the emission of light. Electrons in molecules can only occupy discrete energy levels. They can move up or down these levels, which is called a transition. An electron can transition into another energy state, provided it receives the right amount of energy. This energy is often supplied by light, which can be described by particles - photons - with discrete energy. The energy of a photon is related to the wavelength of light by Planck's constant: $E_{photon} = hf$. Absorption and emission of photons mostly occurs in the lowest electronic energy levels: the singlet ground, first and second excited state (S_0, S_1 and S_2). Thermal energy is not enough to excite an electron from S_0 to S_1, so most electrons reside in the electronic ground state. Once a photon with sufficient energy is absorbed, the electron will transition into S_1 or S_2: its excited state. The absorption takes femtoseconds (10^{-15}, fs).

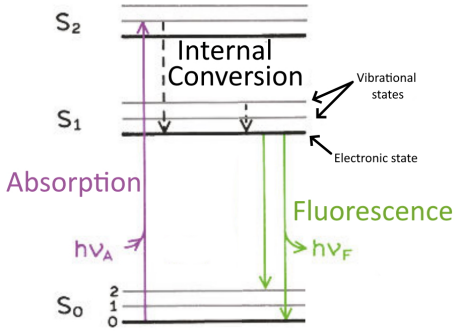

Figure 1.1: Example of a Jablonski diamgram, adapted from [9].

Once a fluorescence molecule is excited, it releases the energy. Within the first 10^{-14} to 10^{-12} seconds, the molecule loses its vibrational energy (within the same excited state) and/or some internal conversion (for instance from S_2 to S_1) takes place. After 1 to 100 nanoseconds (10^{-9} seconds), the molecule can release its remaining energy by emitting a photon and falling back to the ground state. The emission of the photon from an electronically excited state to a lower electronic state is called fluorescence. Generally, the energy of the photon during emission is smaller than that of the absorbed photon, since emission takes place after the molecule has gotten rid of the vibrational energy. The process of absorption, relaxation and emission can be schematically shown in what is called a Jablonski diagram. One such diagram is shown in figure 1.1. There are multiple processes that can occur once a molecule is in the excited state. It need not release a photon for instance, it can also non-radiatively return to the ground state. It can also transition into a different state or react with other molecules.

Fluorophores absorb different wavelengths of light differently, and their emission is also not restricted to just one wavelength. To show how much light of a certain wavelength is adsorbed or emitted, absorption and emission spectra are used. These show the relative absorption and emission intensities at different wavelengths for a given fluorophore. As an example, the spectrum of Alexa Fluor 647 is given in figure 1.2. The large peak in absorption around 650 nm indicates that this fluorophore absorbs photons of that wavelength most efficiently. It can then send out a photon over a whole emission band, but the probability of the emission of a photon with a wavelength of 665 nm is largest.

There are some important parameters related to fluorescence. One of them is the quantum yield (Q), which is a measure of how many photons are emitted compared to how many are absorbed.

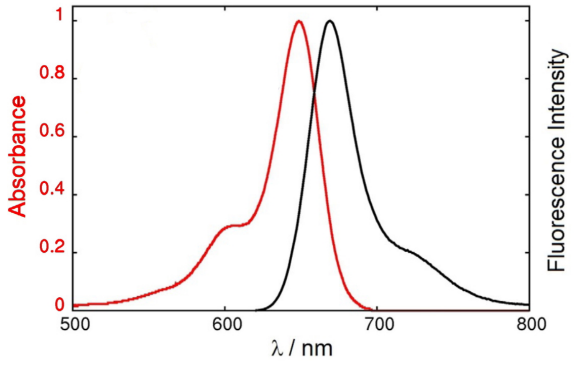

Figure 1.2: Absorption and emission spectrum of AF647, adapted from [10].

This can also be interpreted in terms of rate constants (equation 1.1): k_{nr} is the non-radiative rate constant, indicating how much energy is lost via non-radiative (or dark) decay. k_r is the radiative rate constant, signifying the rate at which photons are emitted.

$$Q = \frac{k_r}{k_r + k_{nr}} \tag{1.1}$$

The rate at which fluorophores decay from the excited state - on average - is the combination of these rates. If on average $k_r + k_{nr}$ events occur per second, then the average time it takes for an event to occur is given by equation 1.2. The fluorescence lifetime (τ) indicates how long an electron or molecule remains in the excited state before it decays back to the ground state.

$$\tau = \frac{1}{k_r + k_{nr}} \tag{1.2}$$

A special case of non-radiative decay is Fluorescence Resonance Energy Transfer, or FRET. Here, two fluorophores with overlap in emission spectrum of one (called the donor fluorophore) and adsorption spectrum of the other (called the acceptor fluorophore) can exchange energy. The donor can transfer its energy non-radiatively to the acceptor, which in turn radiates it. How much energy is transferred depends strongly on the distance r between the donor and acceptor, which makes FRET a suitable to measure intermolecular distances. The transfer rate is given by equation 1.3 and the efficiency by equation 1.4, where R_0 is a measure of how much the absorption and emission spectra overlap and the relative dipole orientation of the fluorophores and τ_D represents the lifetime of the donor in absence of the energy transfer. Due to FRET the donor lifetime is reduced further (or quenched) and the intensity of its emission decreases.

$$k_{fret} = \frac{1}{\tau_D}\left(\frac{R_0}{r}\right)^6 \tag{1.3}$$

$$E_{fret} = \frac{R_0^6}{R_0^6 + r^6} \tag{1.4}$$

A final special case of non-radiative decay is decay via a triplet state. A triplet state is a another excited quantum state, but different from the singlet states: in a triplet state, the excited electron has the same spin as the S_0 state. By the laws of quantum mechanics, decay from a triplet state back into the S_0 state is forbidden, yet is does happen. However, because it is a forbidden process, the rate at which it occurs is very small: orders of magnitude lower than the fluorescence rate. From the excited triplet state, the molecule can again non-radioactively decay in a dark process, or it can send out a photon. The process of emitting a photon from the excited triplet state is called phosphorescence, and can last up to several minutes after excitation. This process can also be included in the Jablonski diagram in figure 1.1, which is shown in figure 1.3. These parameters, specifically the lifetime as well as FRET efficiency, can be collected and used to asses the sample under study.

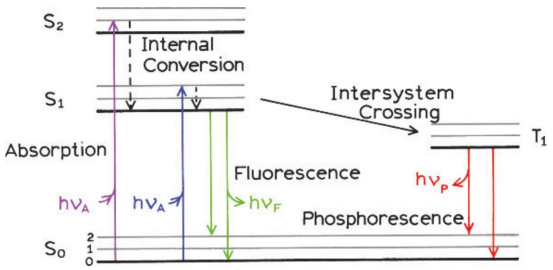

Figure 1.3: Example of a Jablonski diagram that includes intersystem crossing and phosphorescence. Taken from [9].

1.1.1 Pulsed Interleaved Excitation

So far, excitation of a single fluorophore has been described. However, in case of for example FRET the sample is labelled with two fluorophores. For instance, assume the folding of a protein is of interest. To determine the distance between the ends of the protein, one end is labelled with Atto 488 and the other with Atto 565. This labelled sample is diluted to picomolar concentrations to assure single molecule detection. The absorption and emission spectra of both dyes are shown in figure 1.4. The overlap between the emission spectrum of the donor (A488) and the absorption spectrum of the acceptor (A565) between approximately 475-625 nm ensures FRET can occur between these dyes, which makes them suitable for this experiment. In order to perform fluorescence measurements, excitation wavelengths need to be defined. In order to excite the donor, a 488 nm laser will be used. The acceptor will be excited with a 560 nm laser. Note however that the donor excitation wavelength of 488 nm can also excite the acceptor. The 560 nm wavelength used for acceptor excitation cannot excite the donor. The consequence of this fact will be described later.

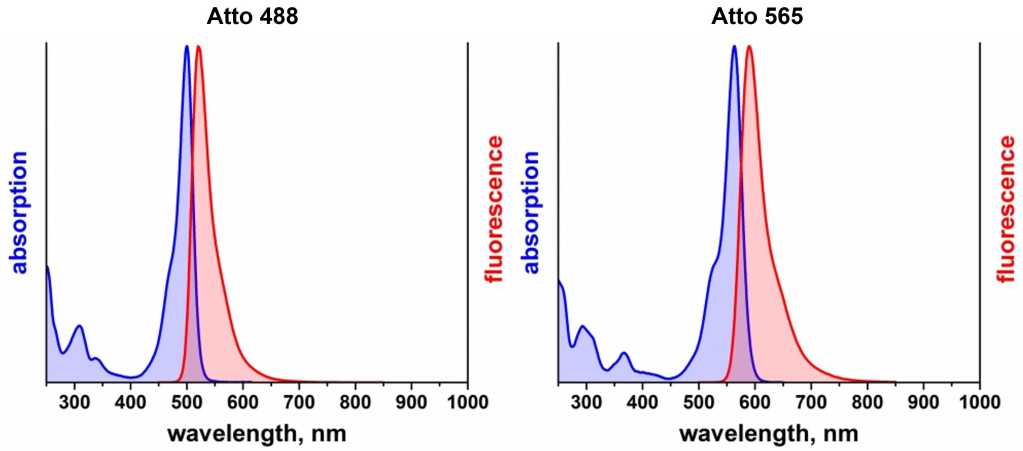

Figure 1.4: Adsoption and emission spectra of Atto 488 and Atto 565. Taken from [11].

During the experiment the emission signal from the donor and acceptor molecules need to be separated. In order to do so, an optical system using dichroic mirrors can be used. These mirrors can reflect one range of wavelengths and let another range pass through (more about the setup will follow in section 2.1). It is important to realize that there are three types of emission of interest: donor emission due to donor excitation (direct donor emission), acceptor emission due to acceptor excitation (direct acceptor emission) and acceptor emission due to donor excitation (FRET). If both lasers were to pulse simultaneously, it is impossible to determine whether an acceptor molecule is excited by the donor laser or the acceptor laser, meaning FRET and (in)direct acceptor emission cannot be discriminated. Therefore, the lasers need to pulse alternatively. Additionally, the time between pulses must be much smaller than the diffusion time of the molecules,

otherwise the molecule might leave the detection volume before the second pulse can excite the fluorophores. This method of rapid interleaved pulses is called Pulsed Interleaved Excitation, or PIE. In this case, the lasers alternate at a frequency of 40 MHz.

A schematic of the processes that follow the donor excitation pulse is included in figure 1.5. The laser is directed into the sample where it excites the donor fluorophores. The donor emission travels through the series of dichroic mirrors to detector 2. In case of FRET, the excited donor transfers its energy to an acceptor which emits it. This FRET emission is separated from the donor emission by the dichroic mirrors and ends up in detector two. Because the 485 nm laser can also excite the acceptor, some indirect acceptor emission also ends up in the first detector. After a very short time (25 ns) the second pulse of the 560 nm laser is send out. This is shown in figure 1.6. It is also directed into the sample where it only excite the acceptor molecules. This direct acceptor emission is then fed into the first detector, exactly like the indirect acceptor emission during the donor excitation pulse. The process will then repeat for the duration of the measurement during which the detectors will record exactly what laser gave off a pulse at what time and how long it took for the photons to arrive.

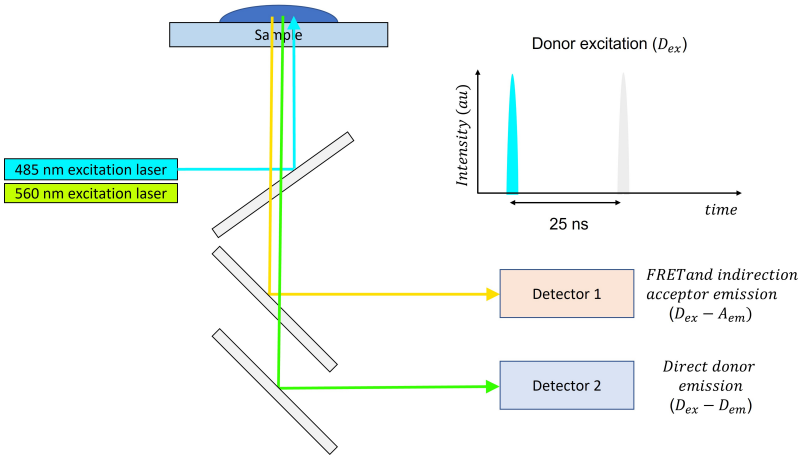

Figure 1.5: Schematic of the setup and the emission processes during the 485 nm pulse for donor excitation.

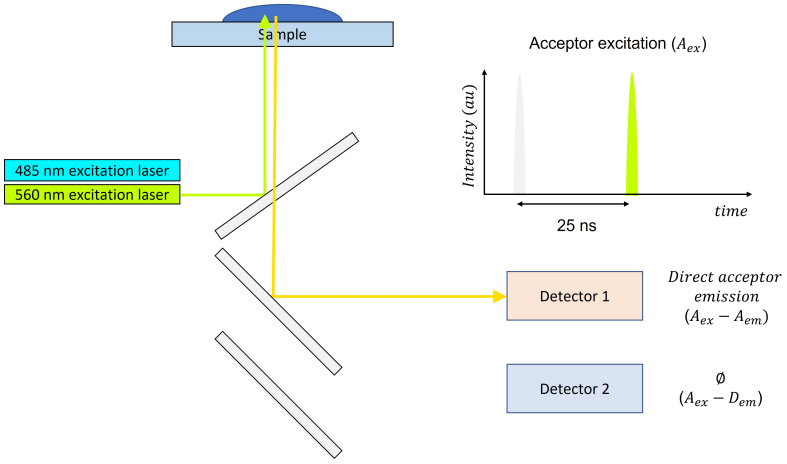

Figure 1.6: Schematic of the setup and the emission processes during the 560 nm pulse for acceptor excitation.

Once all the data is collected, the indirect acceptor emission signal needs to be separated from

the FRET emission signal. Since both the donor and the acceptor need to be present in the detection volume for FRET to occur, separation can be achieved by identifying all intensity bursts in the $D_{ex} - A_{em}$ signal that coincide with direct donor bursts in the $D_{ex} - D_{em}$ signal. Any other acceptor emission during donor excitation is classified as indirect acceptor excitation. After this is established, further analysis into for instance FRET efficiency can take place. Alternatively, other type of measurements like life time measurements, FCS or TCCD (see sections 1.1.2, 1.1.3 and 1.1.4 respectively) can be performed using much the same process as described here.

1.1.2 Lifetime measurements

Using the data that the detectors store for each signal they receive, the fluorescence lifetime τ can be determined. Shortly after the excitation pulse there exists a certain amount of fluorophores in the excited state $n(t)$ which varies with time. How much the amount of excited fluorophores changes with time can be described using the rate constants. If one fluorophore decays with on average $k_r + k_{nr}$ events per second, then n fluorophores decay with:

$$\frac{dn(t)}{dt} = (k_r + k_{nr})n(t) \tag{1.5}$$

This differential equation can be solved, which results in equation 1.6.

$$n(t) = n_0 \exp\left(-t(k_r + k_{nr})\right) = n_0 \exp\left(\frac{-t}{\tau}\right) \tag{1.6}$$

As the intensity signal that is measured is proportional to $n(t)$, it also holds that

$$I(t) = I_0 \exp\left(\frac{-t}{\tau}\right) \tag{1.7}$$

The measured intensity over time after the excitation pulse can be plotted and fitted with the model in equation 1.7. This will allow for the determination of the lifetime τ. In multi-component systems, the model extends to:

$$I(t) = \sum_i I_0^i \exp(-t/\tau_i) \tag{1.8}$$

A way in which lifetime can be measured is using Time Correlated Single Photon Counting (TCSPC). TCSPC measurements require lasers with short pulses (often pico or femtoseconds) and high repetition rates (MHz) which send very short pulses into the sample. The conditions are such that per pulse, less than one (often 1/100) emission photon is detected. The time between the excitation pulse and the arrival of the emission photon is measured. After many photons have arrived at the detector, a histogram can be created. This technique allows for better time resolution than what would be observed when many fluorophores are excited at the same time. Figure 1.7 shows this process schematically.

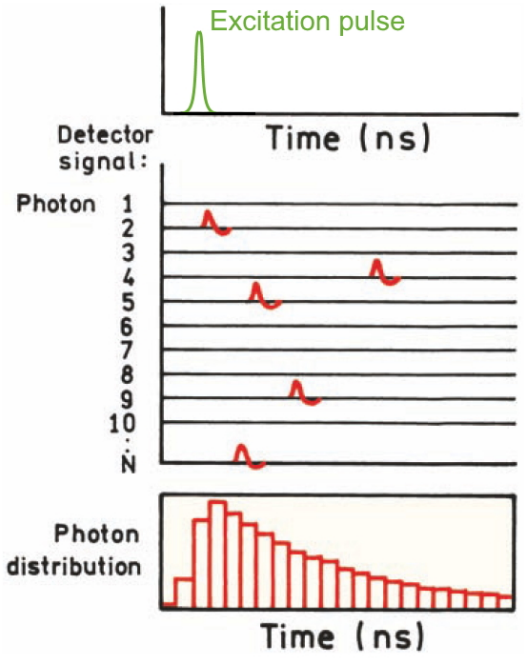

Figure 1.7: Schematic of the TCSPC process. Adapted from [9].

1.1.3 Fluorescence Correlation Spectroscopy

One of the ways in which fluorescence can be used to gain information about a sample is by using Fluorescence Correlation Spectroscopy, or FCS. FCS relies on time correlation of the fluorescence emission signal to find the average amount of molecules in the detection volume ($< N >$) and the residence time or diffusion time (τ_d) from the time trace fluctuation. If the shape and size of the observation volume are known, then the diffusion constant of the molecule D can be inferred from the volume and τ_d. In contrast to TCCD or FRET, FCS is not limited to single molecule samples.

In FCS, laser light is focused into a sample with a certain concentration of molecules C. The volume illuminated by the laser is called the detection volume V_{det}. Fluorophores present in this volume can absorb one of the photons supplied by the laser, which may or may not allow them to fluoresce. The higher the concentration of molecules in the sample, the more molecules one can expect in the detection volume and the higher the fluorescence emission. For a given combination of V_{det} and C, one can calculate the expected number of molecules in the detection volume $< N >$, say that $< N >= 1$. Since this concerns an average, the actual number of molecules in the detection volume could also be for instance zero or two. This variation[1] causes fluctuations in the detected emission intensity signal, where the speed at which the molecules diffuse (the diffusion constant) through the detection volume determines the rate of variation, as can be seen in figure 1.8. The diffusion constant is related to the diffusion time by equation 1.9[2]. ω is related to the focus of the laser and is given by equation 1.10 where V_{eff} is the effective detection volume obtained through calibration and κ is a parameter related to its geometry.

$$D = \frac{\omega^2}{4\tau_d} \tag{1.9}$$

$$\omega = \left(\frac{V_{eff}}{\kappa}\right)^{1/3} \pi^{-1/2} \tag{1.10}$$

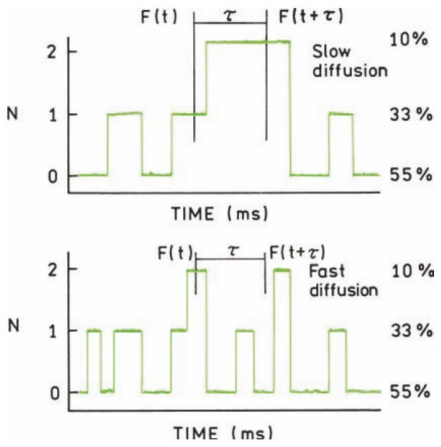

Figure 1.8: Fluctuations in the number of fluorophores (N) in the observed volume of 1 fl with c = 1 nM. The intensity axis is in units of the intensity from a single fluorophore. Caption and figure taken from[9].

Since both of these parameters - $< N >$ and τ_d - are captured in the nature of the intensity trace, it is possible to retrieve them from the data. This can be done using correlation, which can be described as quantifying the similarity of the signal with a version of itself, some time τ in the future. If the fluorescence signal as function of time is given by $F(t)$, then the autocorrelation function $G(\tau)$ of $F(t)$ is given by equation 1.11 [9].

[1] Additionally, the intensity within the detection volume varies which causes additional variation. Here, an ideal detection volume - which has a homogeneous distribution of intensity - is assumed for simplicity.

[2] As defined by SymPhoTime64 software of the FCS setup

$$G(\tau) = \frac{1}{T}\int_0^T F(t)F(t+\tau)dt \tag{1.11}$$

The actual description of $G(\tau)$ depends on how the system behaves: specifically on what the mode of diffusion is. For pure diffusion, one will find equation 1.12, where $G(0) =< N >^{-1}$. Fitting this model to the autocorrelated data yields the value of $< N >$ and, provided the geometry of the detection volume is known, the diffusion constant D. The information about the detection volume can be found by calibrating known samples.

$$G_D(\tau) = G(0)\left(1+\frac{\tau}{\tau_d}\right)^{-1}\left(1+\left(\frac{\tau}{\tau_d\kappa^2}\right)\right)^{-1/2} \tag{1.12}$$

If the fluorophore gets excited into the triplet state, it is not observed (provided that the fluorophores have left the detection volume before transitioning back to S_0). This decreases the emission signal and increases the correlation amplitude. If the fluorophores do transition from the triplet state back to S_0 within τ_d, or a fluorophore previously excited to the triplet state diffuses back into the detection volume and emits a photon, then this causes an additional fluctuation in the signal apart from regular fluorescence. This is referred to as (fluorophore) blinking. Blinking will create an additional component in the correlation curve: $G(\tau)$ will now be the product of the correlation due to diffusion ($G_D(\tau)$) and the correlation due to the triplet state transition ($G_T(\tau)$), where $G_T(\tau)$ is given in equation 1.14 where f_T is the fraction of molecules in the triplet state and τ_T is the relaxation time for the triplet decay [9].

$$G(\tau) = G_D(\tau)G_T(\tau) \tag{1.13}$$

$$G_T(\tau) = 1 + \frac{f_T}{1-f_T}exp\left(-\frac{\tau}{\tau_T}\right) \tag{1.14}$$

The measurements in this research will mostly rely on FCS, specifically the qualitative behaviour of the correlation function, to asses the effect of the ZMW. Once this is established, focus will shift to a different type of measurements: Two Colour Coincident Detection, or TCCD measurements. These will be explained in the next section.

1.1.4 Two Colour Coincident Detection

A different way to measure fluorophores in single molecule detection mode is Two Colour Coincident Detection (TCCD). TCCD probes two reactions partners (A and B) labelled with one dye (for example A-A488 and B-A565). A and B are dissolved in small concentrations to obtain single molecule events and mixed together in some ratio. Some of A and B will react to AB and some fraction A and another fraction B remain. This sample is then put on an FCS setup similar to the one described in section 1.1.1.

If AB diffuses into the detection volume, it will give off a intensity burst in both detection channels coincident in time. If only A or only B diffuses through, this will lead to only a burst in the corresponding detection channel. If both A and B happen to diffuse through the detection volume at the same time - while not being bound - they will also produce bursts in both channels. The number of events related to the random coincident detection of A and B can be estimated, such that the number of events due to AB can be compared to the total number of detected events. The association quotient Q in equation 1.15 can be defined, where r_C is the rate (photons/sec) of coincident (non-random) events due to AB and r_A and r_B are the rate of events due to only A or B. r_C can be defined as $r_C = r_S - r_R$, where r_S is the total rate of simultaneous events (both by coincidence as well as by AB) and r_R is the rate at which A and B coincide randomly. This gives insight in how much of A and B has reacted, as shown by [[12], [13] and [14]], among others.

$$Q = \frac{r_C}{r_A + r_B} \tag{1.15}$$

1.1.5 Limitations of fluorescence measurements on single molecules

When using the fluorescence methods described in this chapter there are some factors one should take into account, especially when single molecule analysis is performed. The biggest problem facing single molecule detection is the upper limit on the concentration of the sample. When investigating dynamics or aggregation mechanisms, the contribution of only one molecule at a time needs to be detected. It is easy enough to identify that contribution if on average only 1 or 2 molecules reside in the detection volume, but finding the contribution of one molecule when on average 100 or even 1000 of them are detected quickly becomes impossible. In order to maintain a small number of molecules in the dectection volume, one can reduce the size of the detection volume. However, the size reduction is limited by the diffraction limit of light. In conventional confocal setups the minimum detection volume often lies in the femtoliter (10^{-15}) range [[7], [8]]. To obtain single molecule occupancy in the detection volume, the maximum concentration of the sample is limited to the picomolar to nanomolar ($10^{-12} - 10^{-9}$) range. However, in order to accurately determine for instance dissociation constants of biomolecular interactions, concentrations in the micromolar to even milimolar ($10^{-6} - 10^{-3}$) range [15] are required (see figure 1.9).

A second challenge related to the size of the detection volume arises when single molecule detection is actually achieved. A single molecule on its own produces only so much emission signal. This means special care should be taken to reduce any noise (from scattering to dark counts) to a minimum in order to discriminate the emission from the background signal. The ratio between signal strength and background noise is called the Signal to Noise Ratio (SNR). As explained by Holzmeister at al. [15], the signal of a single molecule (in first approximation) does not depend on the size of the detection volume, but the background signal - including Rayleigh or Raman-scattering - does increase with larger volumes: thus, there is a relatively large amount of 'noise emitters' and only few fluorescence emitters in a conventional observation volume, which means that capturing enough data to statistically analyse it can require hours of acquisition time. This is not as much a limitation as it is a challenge, because collecting single molecule data is still possible provided the setup is stable enough.

One last limitation worth noting concerns itself with nanosecond dynamics.When investigating dynamics, data cannot be collected faster than the rate at which photons are emitted by the fluorophores. Practically, that means that events shorter than approximately 20 nanoseconds [16] cannot be registered. This limitation cannot be circumvented by reducing the detection volume: it is more technical in nature. In order to increase the time resolution, fluorophores must be quenched more strongly without the loss of quantum yield. As it turns out, zero-mode waveguides pose a solution to not only this limitation but also to the other issues raised in this section. The following section will introduce these waveguides.

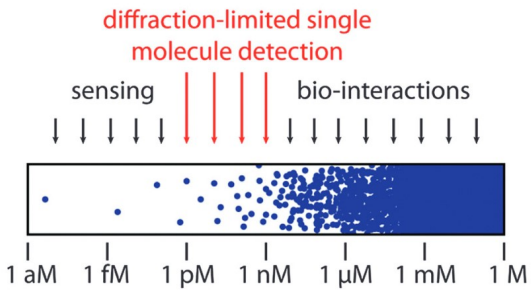

Figure 1.9: Single-molecule experiments are feasible in a narrow concentration range between pM and low nM. Protein interactions and enzymatic activity often require concentrations larger than mM. Caption and figure adapted from [15].

1.2 Zero-mode waveguides

In order to circumvent the problems relating to detection volume and time resolution in fluorescence methods described in section 1.1.5, multiple solutions exist. The use of zero-mode waveguides (ZMWs) is just one of multiple (nano) mechanical ways. In essence, ZMWs are nothing more than holes pierced in a metal film. Levene et al. [17] were the first to show what these seemingly simple structures are capable of: back in 2003, they reported arrays of ZMWs to be "a simple and highly parallel means for studying single-molecule dynamics at micromolar concentrations with microsecond temporal resolution". Since then, many articles have surfaced investigating different molecules, concentrations, materials, shapes, sizes and more. The power of ZMWs lies in i) the (mechanical) reduction of the detection volume by the metallic aperture, ii) the enhancement and localization of the excitation field and iii) the interactions of the fluorophores with the metal. This section will elaborate on these effects further.

Field enhancement, localization and quenching

The diameter of a confocal detection volume is typically a couple hundred nanometers. When reduced with a ZMW, only tens to at most two hundred nanometers are all that remain: too small for light to propagate through. Hence the name zero-mode waveguide: it is a waveguide in which no - i.e. zero - propagating modes exist. Inside ZMWs, there only exists a rapidly decaying evanescent field. At a scale smaller than the wavelength of light, spatial variations in the electric field of the light exists inside these structures. The metal that the ZMW consists of contains free electrons, that can move collectively due to these local variations [[18], [19]]. These oscillations are referred to as surface plasmons. When the plasmons are induced optically, they are referred to as surface plasmon polaritons (SPPs). For the course of this report, they are referred to simply as 'plasmons'. The plasmons are not confined to a specific region: they can propagate through the metal and resonate with the electric field of the incident light, enhancing the field. Figure 1.10 shows the distribution of the electric field in pyramidal shaped aperture with an approximately 40 nm sized square hole in the middle. Light is incident on the bottom of the hole and the colours indicate the intensity distribution. Note that the intensity at the top of the pyramid (left hand side) reaches a maximum of about 80 au, while the plasmons were only excited down the hole: the plasmons have travelled up to the top and locally enhanced the field there.

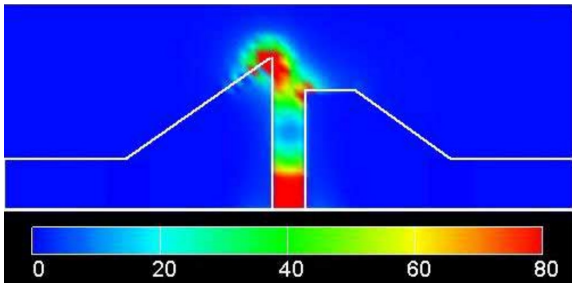

Figure 1.10: Numerical simulation of the field enhancement due to a nanostructure, taken from [20] .

There is more to these nanostructures than enhanced excitation emission: they also interact with fluorophores in their vicinity [18]. Non-radiatve energy transfer can occur between an excited fluorophore and the plasmons in the metal. The fluorophore will be quenched, but the plasmons can still radiate the energy into the far field by emitting a photon. If the quantum yield of the plasmons is equal to or greater than that of the fluorophore, the efficiency does not decrease - it might even increase - while the fluorophore is quenched. Not only can the fluorophore be re-excited faster, allowing for more radiative events per unit time, there might also be more photons emitted in general because the quantum efficiency of the system (ZMW with fluorophore) is larger than that of just the fluorophore alone. Therefore, higher emission signals can be obtained and dynamics

at lower time scales can be investigated.

Adsorption

However, there is a substantial challenge involved in the use of ZWMs: preventing the molecules in the sample from adsorbing to the surface of the glass or the metal. Not only will this decrease the effective concentration of the sample, it will also create artifacts in the data, specifically when dealing with ZWMs compared to open solution. One of the problems created by adsorption is the change in diffusion time: because the molecules adsorb to the surface they remain in the detection volume longer. This causes their diffusion time to increase and prevents an accurate determination of the diffusion constant. Secondly, if a molecule remains in the detection volume too long, it might be excited and re-excited more often, increasing the emission signal. This makes discrimination of single molecule events more difficult: it will not be possible to tell whether the burst in intensity is due to one molecule that is there a long time, or to two or three molecules coming in shortly after each other. This affects for instance the association quotient described in section 1.1.4.

A seemingly simple solution to prevent molecules in the sample from adsorbing to the surface of the waveguides is passivating it. This can be done by taking some other molecule (a passivation agent) and cover the surface with it before conducting the measurements. The passivation agent can bond to the surface by any means: electrostatically, covalently or even by Vanderwaals forces. Regarless of the adsorption mechanism, its purpose is the same: blocking adsoption sites on the surface from being occupied by the sample molecules under study. However, this process is more complicated than it seems. Not every molecule adsorbs to glass and/or aluminium, and not every passivation agent prevents adsorption of just any molecule. Patra et al. performed a study in 2020 [21] to benchmark the effectiveness of various passivation agents. They created aluminium ZMWs with a diameter of 110 nm in a 100 nm thick aluminium layer and measured various red and green Atto and Alexa Fluor dyes (A550, AF546, A647N and AF647). Some of these, the Atto dyes in particular, seemed to adsorb strongly: evident by the increased average number of molecules and the diffusion time, as well as the behaviour in the time trace. They then performed passivation protocols with various passivation agents, like silane-modified Poly Ethylene Glycol (PEG) with different molecular weights, poly(vinyl)phosphonic acid (PVPA) and bovine serum albumin (BSA) and reassessed the results. PVPA and PEG with a molecular weight of 1000 Da were reported to perform best (see also figure 1.11), whereas the data collected using BSA-passivated ZMWs still showed evidence of adsorption.

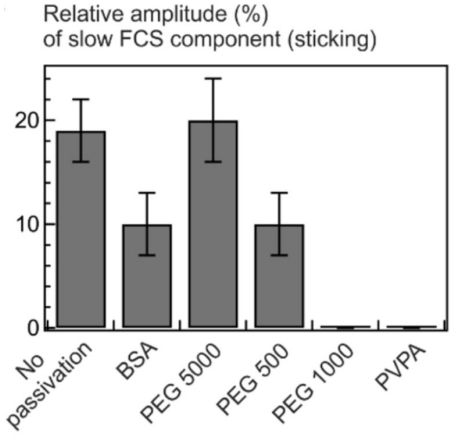

Figure 1.11: Relative amplitude of the slow diffusion component for different ZMW surface passivations. Caption and figure taken from [21].

They also provided the tail-tell signs of surface adsorption in both FCS and time trace data (figure 1.12). When the sample adsorbs, the amount of counts per unit time increases, as does

the average number of molecules. The fluctuations in the time trace data occur at longer time scales, which results in an additional FCS-component for longer (>1 ms) lag times. The adsorbing sample (A647N-DNA) did not show these signs after the surface of the ZMWs has been treated with either PVPA or PEG.

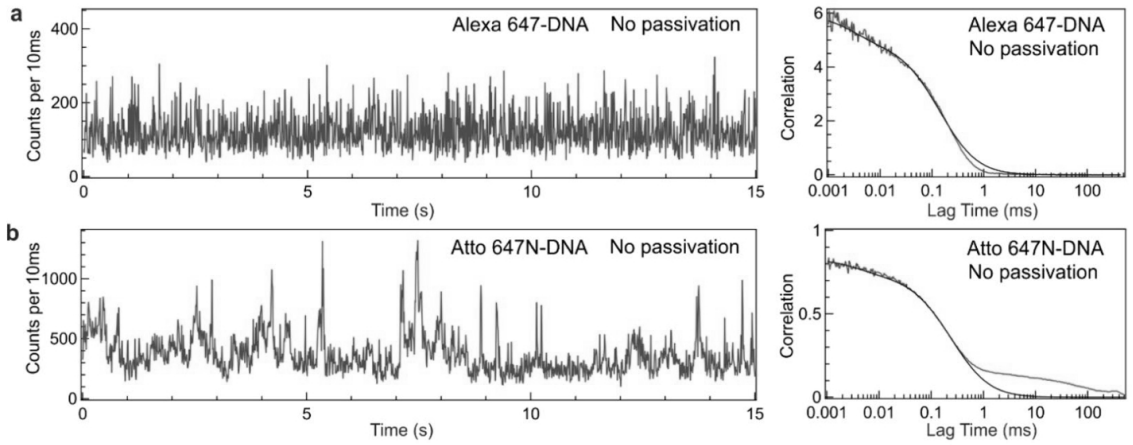

Figure 1.12: Time trace data and FCS data for two different fluorophores. (a) shows AF647-DNA, which does not adsorb. (b) shows A647N-DNA, which does adsorb. Adapted from [21].

Other authors that have successfully performed FCS with similar samples as the ones aimed for in this research (DNA [22] and peptides [16]) have also opted for PEG-1000 as passivation agent. Unfortunately, everything that was at hand during the first stages of this research was BSA. Early experiments will therefore show passivation experiments with either BSA and/or other improvised compounds.

To conclude: due to the reduced observation volume inside the ZMW, larger concentrations can be used for single molecule measurements. Additionally, the field localization and enhancement as well as the quenching of fluorophores - both courtesy of the interaction with surface plasmons - increase fluorescence signal, allowing for higher signal and reduced data acquisition times. Finally, the faster radiative rate of the fluorophores opens possibilities to detect dynamics nanosecond timescales previously inaccessible by regular FCS, as well as reduction of data acquisition times. This makes ZMWs one of the more promising methods to obtain single molecule measurements with moderate to high sample concentrations.

Chapter 2

Methods

This chapter will explain the setup used for the fluorescence measurements and the protocols regarding the passivation and the data collection. Lastly, it will explain the way in which the data is analysed.

2.1 FCS setup

In order to perform FCS, TCCD or TCSPC measurements, the PicoQuant MicroTime 200 setup is used. It houses four different excitation lasers (405, 488, 560 and 640 nm) which can be used for the fluorescence measurements. This section will briefly explain the optical system of the PicoQuant.

Excitation

After selecting (one of) the excitation wavelength(s), it needs to be directed towards and focused into the sample. To this end a mirror and an objective (Olympus UplansApo 60x 1.2W 0.3-0.21 FN26.5) can be used. The tighter the focus, the smaller the detection volume of the FCS setup. Additionally, optical attenuation filters to control the laser power can be installed as well as a compensator, which can be used to center the laser beam to make it as symmetric as possible. Additionally, a beam splitter and camera can be installed to aid in focusing the light into the sample.

Emission

Once the fluorophores are excited and fluorescence occurs, the emission and the excitation light reflected from the glass-water interface travel back through the objective. In order to separate them, a dichroic mirror is used. Such a mirror reflects a specific band of wavelengths and allows another band to pass through. The emission light will travel down the optical system further, where it encounters a pinhole. To restrict the detection volume further, a pinhole is used that only passes signal form a selective volume in the sample. Further filtering or beam splitting can take place with a selection or bandpass or longpass filters before the emission is led into the detector (Excelitas Single Photon Counting Module detectors (SPCM-AQHR-14-TR)). The details regarding the exact optical system for the various measurements has been included in the appendix (section A.3).

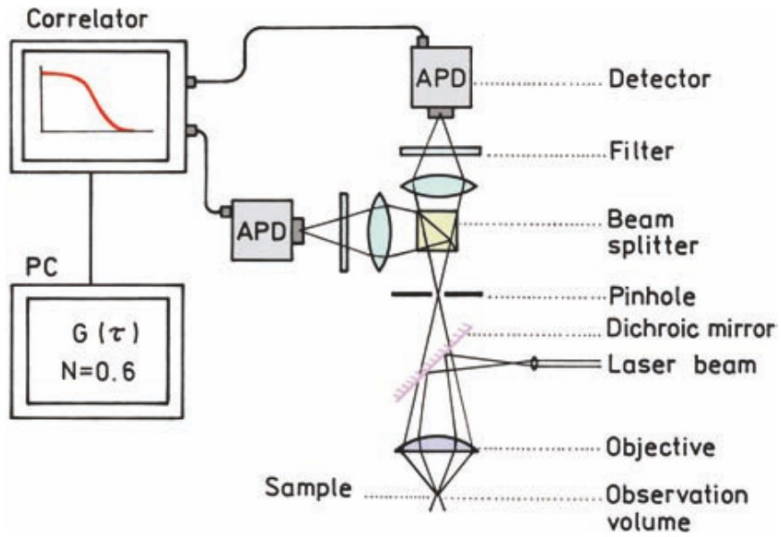

Figure 2.1: Schematic representation of a basic two-channel FCS setup. Taken from [9].

2.2 Passivation protocols

The passivation protocol for all passivation agents was similar throughout the experiments. First, the aluminium coated coverslips containing the ZMWs were rinsed with MilliQ water to remove any dust. Next, the coverslips were cleaned in air plasma (CUTE plasma system, see section A.2) for 5 minutes to remove any organic compounds adsorbed to the surface. After cleaning, the coverslips where either deposited in a solution containing the passivation agent.

For PEG passivation, 1 mg/mL of PEG was dissolved in a solution of absolute ethanol with 1% acetic acid. The cleaned coverslips with the waveguides are left to incubate in that solution for at least 12 hours, as described by [16], [21],[22]. The incubation took place in a custom made nitrogen enclosure. After incubation, the coverslips were rinsed with 70% ethanol and dried in nitrogren to remove access PEG solution. They were stored in air.

For other passivation agents (BSA, AF488, aSyn-WT and unlabelled DNA) a 30 μL drop of 5 μM passivation solution was deposited on the coverslips and they were left to incubate for 5 minutes in air. After incubating the coverslips, there were rinsed with MilliQ to remove excess passivation solution and dried using nitrogen. The coverslips are then stored in air.

2.3 Measurement procedure

For each measurement in a ZMW, the procedure was as follows. First, the FCS setup was calibrated to make sure the optical system was aligned properly. The right optical filters (see section A.3) were inserted along with the right dichroic mirror and the laser power for the excitation lasers was set accordingly. The coverslips with ZMWs were placed on the sample holder and the waveguides were located using a confocal microscope. 30 μL of sample solution was deposited on the coverslip after which a 2D scanning image was made, showing diffraction limited spots where the waveguides are. While measuring the time trace, the diffraction limited spot was manually scanned in the lateral direction until burst became visible and the number of events per ms was maximum. This indicated that the ZMW was found and that the lasers were focused properly. Immediately after, a measurement was started, allowing for TCSPC, FCS and time trace data to be collected.

2.4 Data analysis

Number of molecules and diffusion time

Using the collected data, the expected number of molecules in the detection volume $< N >$ and the diffusion time τ_d can be determined. As described in section 1.1.3., a model can be fitted to the data which returns the values of $< N >$ and τ_d. Figure 2.2 shows an example using AF488 dye. A triplet model (equation 1.13) returns the values of interest: in this case, the average number of molecules $< N > \approx 2.6$ and the diffusion time is found to be $\tau_d \approx 0.05$ ms.

However, fitting this model becomes challenging when ZMW are used to measure single molecules. For one, because the model assumes a certain geometric volume through which the molecules diffuse. Inside the ZMW, this assumption does not hold true. Additionally, the burst traces acquired when using ZMWs do not contain a lot of data to base the correlation on: in open solution, burst traces can be measured anywhere from 30 minutes to multiple hours, allowing for sufficient events to derive the FCS data from. However, the system with the ZMW is by far not stable enough to perform such long measurements. The evanescent field inside the waveguide decays exponentially, so the focal plane needs to be as close to the bottom of the waveguide as possible: within a couple tens of nanometers the field has decreased too much for any detectable signal to be produced, despite the enhancement the waveguide provides. The combination of these factors made it such that none of the standard diffusion models (pure diffusion, triplet, extended triplet, etc.) could be reliably fitted. To illustrate this, an FCS measurement with DNA in a ZMW has been included in

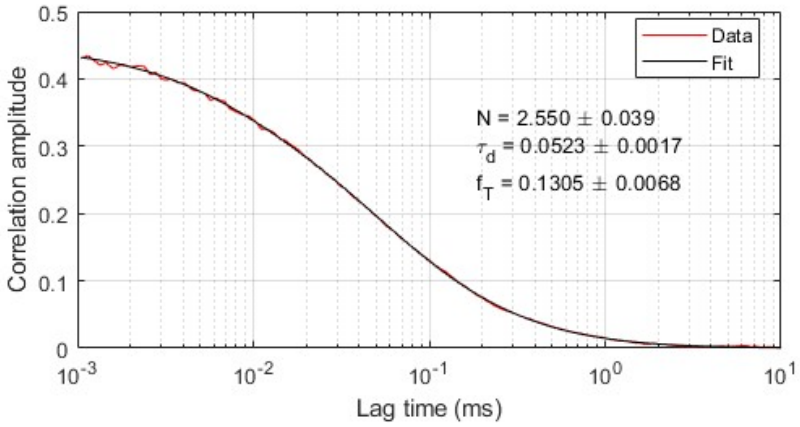

Figure 2.2: FCS measurement (data and fit) of AF488 dye measured at 2 nM in open solution.

figure 2.3.

The data in figure 2.3 has also been fitted with the triplet diffusion model from equation 1.13. At first glance, the data from the direct donor emission seems reasonable. However, a very high triplet fraction of 0.986 results in an almost unreasonable number of molecules in the detection volume. If we take the detection volume to be an attoliter ($10^{-18}L$) - the expected value based on literature - then the concentration with 122 molecules in that volume would be over 200,000 nM. That is over 2000 times higher than the actual concentration used (100 nM). Furthermore, the diffusion constant seems very small, but not out of place. The diffusion time in open solution is in the range of 0.1-0.2 ms and its ZMW counterpart is expected to be much smaller. The same reasoning holds for the diffusion time obtained from the direct acceptor data. In the case of the direct acceptor, no average number of molecules can be defined: the model returns a NAN value. This is because the triplet fraction - which by definition lies between 0 and 1 - is found to be 3.1. Since the number of molecules is defined as $< N >= 1/[(1 - f_T)(\rho)]$, where ρ corresponds to the amplitude of the correlation function, this would result in a negative number of molecules in the detection volume which is nonphysical.

Another example of the results of the fit of the triplet model on ZMW data is given in figure 2.4. Here, a different sample (double labelled aSyn) has been used. The problem with the model is complementary to that in case of double labelled DNA (figure 2.3): the parameters provided by the model are completely reasonable, yet the model does not fit the data properly. Only the domain between 10^{-2} and 10^{3} ms shows a decent fit. The data in the microsecond regime does not get fitted properly, even though the model detects a triplet state: this begs the question how reliable the determined values for the triplet fraction and in turn the number of molecules really is. Using this diffusion model is thus not a reliable way to obtain the parameters of interest. The same problems occur for any of the other diffusion models - pure diffusion, extended triplets, etc. All of them do not provide consistent or reliable parameters.

To circumvent this problem and to speed up data analysis a solution is created which will be explained based on the example shown in figure 2.4. From the figure, it is clear that the model fits the data reasonably will for lag times larger than 10^{-2} ms. Presumably, there exists some microsecond process on top of the triplet transition that the current models do not take into account, so it has been decided to ignore the correlation data in that regime and only focus on the correlation related to lag times larger than 10^{-2} ms. However, clipping the data will not resolve the issue related to the quality of the fit. Unfortunately, the regular process of fitting a model does not work so instead unfitted data will be used. The diffusion time will be determined by locating the point at half max ($G(\tau_d) = \frac{1}{2}G(0)$, which will results in $\tau_d = 0.8983$ ms in the example in figure 2.4. This matched the diffusion time obtained through the model, which gives some support to this technique. The number of molecules will be determined the correlation value at $G(\tau = 10^{-2})$.

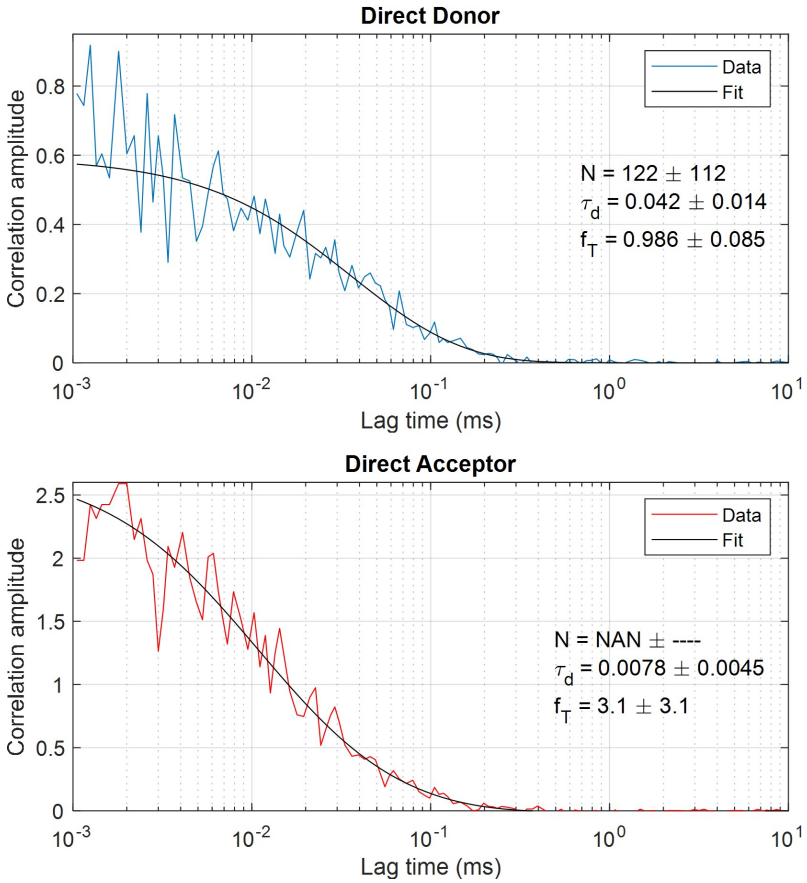

Figure 2.3: FCS measurement (data and fit) of 100 nM double labelled DNA A488-A565 sample measured inside a ZMW.

Using this process, the amount of molecules is $N \approx 1/14 \approx 0.07$. This will yield concentrations much closer to 110 nM, which is a reasonable value.

Count rate per molecule and enhancement factor

Finally, the count rate (CR) is defined as the average of the time trace. As the time trace data provides the events per millisecond, the count rate is the average amount of events per ms. This value depends on the concentration: the higher the concentration, the more molecules in the detection volume and the higher the signal. By design, the ZMW has less molecules in the detection volume than a measurement in open solution with the same concentration. Therefore, the CR in a ZMW will always be lower than that in open solution, which makes the CR unsuitable to compare such experiments. To solve this, the CR can be normalized by the number of molecules in the detection volume. This yields the count rate per molecule, or CRM in $(average\ events) \cdot ms^{-1} \cdot (molecule)^{-1}$. This value can be used to compare emission signal in open solution with the ones in ZMWs: if the CRM_{ZMW} in the ZMW is divided by the CRM_{OS} in open solution, the fluorescence enhancement $\eta = CMR_{ZMW}/CRM_{OS}$ is obtained.

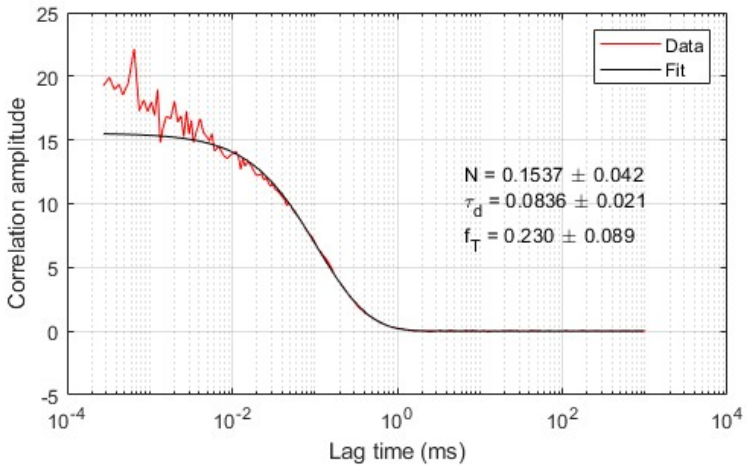

Figure 2.4: FCS measurement (data and fit) of 50 nM double labelled aSyn AF568-AF647 measured inside a ZMW. The FCS data corresponds to direct acceptor emission.

Chapter 3

Design and fabrication of zero-mode waveguides

There are various aspects related to the design of ZMWs. One of the important concepts to take into account is the degree to which fluorescence signal is enhanced. This is a consequence of how the plasmons interact with the fluorophores. Multiple studies, including but not limited to Foquet et al. [23], Rigineault at al. [24] and Wenger et al. [25] have investigated the effect of the size of the waveguides on fluorescence enhancement and lifetime quenching. Others, like Gérard et al. [26], explicitly compared the difference between metals. Apart from them, there are authors not explicitly investigating parameters, but simply reporting enhancement with some combination of ZMWs, production techniques and fluorophores. This chapter will discuss the these design choices, fabrication techniques and the validation experiments of the prototype ZMWs for measuring biomolecular interactions, with specific focus on aSyn.

3.1 Design parameters

How to design the ZMWs will be divided into three parts. First, we consider the backbone of the waveguide: the metal cladding. Commonly used are gold and aluminium. The metal layer must be 'optically dense', i.e. no light must propagate through it. Therefore, highly reflective metals are good candidates. The relative reflection of a metal depends on the wavelength of the light. In figure 3.1, this dependency is shown for some metals. Within the visible region of the spectrum - the region in which the excitation and emission wavelengths of the fluorophores lie - we find silver, aluminium, copper and gold as most reflective metals. Due to its vast variety in reflection over the wavelength region of interest, copper is excluded from the list of possible metals. Silver is reported to oxidize and blacken during measurements [27] and therefore unsuitable, leaving only gold and aluminium. Gold, being a noble metal, is not prone to oxidation. However, it only provides decent reflectivity for wavelengths over 500 nm. Aluminium reflects relatively consistent over the visible wavelength range. It does oxidize, but it forms only a small layer of aluminium oxide halting the oxidation process. Since dyes with excitation wavelengths lower than 500 nm (AF488 specifically) will also be used, aluminium was chosen as the metal in which the ZMWs will be made.

Secondly, the layer thickness is investigated. Based on the consulted literature, the layer thickness of a ZMW is often between 100 and 300 nm thick (see table 3.1). Foquet et al. [23] reported that the minimal layer thickness for aluminium in order to have a 'decent SNR' is 100 nm, with increasing SNR the thicker the layer. However, the thicker the layer, the less likely it is a molecule will diffuse all the way down to the detection volume. It was decided the ZMWs for this research would be made in 150 nm thick aluminium, halfway in the range of what other authors have reported.

The third and last component of the design is the question of waveguide diameter. Since the ZMW is a circular waveguide, a cut-off frequency or wavelength can be defined: the maximum

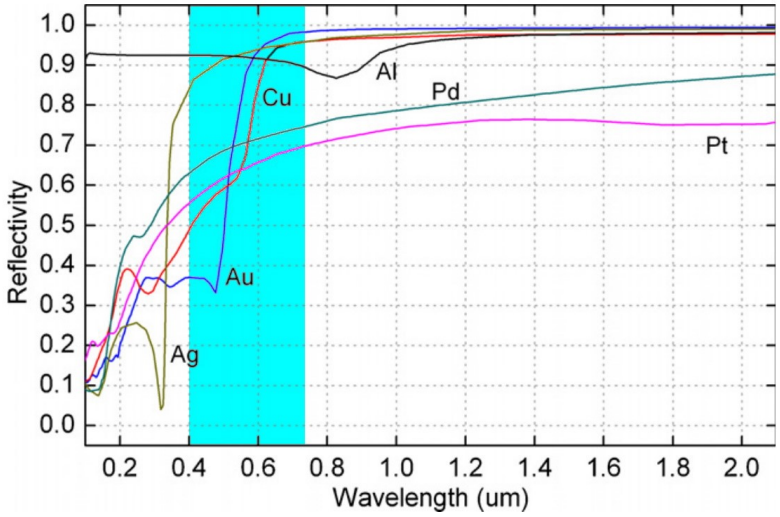

Figure 3.1: Reflectivity of various metals as a function of wavelength, adapted from [28]. The shaded region indicates the visible spectrum.

Comparison of various 'classical' ZMWs						
Author	Metal	Thickness (nm)	Diameter (nm)	Excitation wavelength (nm)	Dye	Citation
Nüesch 2022	Aluminium	100	120	488	AF488 AF594	[16]
Patra 2020	Aluminium	100	110	557 635	A550 AF546 A647N AF647	[21]
Foquet 2008	Aluminium	100-170	40-150 50-110	488	AF488	[23]
Rigeault 2005	Aluminium	300	110-420	488	Rh6G	[24]
Gérard 2008	Aluminium Gold	200	80-310	633	AF647	[26]
Wenger 2008	Gold	200	80-310	633	AF647	[25]

Table 3.1: Overview of various waveguide diameters, wavelengths and dyes found in literature.

diameter d_c[1] that can be used for an excitation wavelength λ_{ex} is given by $d_c = \lambda_{ex}/1.7$ [6], [17]. Practically, that means the maximum diameter of the waveguide must be somewhere between 287 nm and 376 nm, assuming excitation wavelengths between 488 nm and 650 nm .

To find the optimal diameter within this range, Wenger et al. [25], investigated the effect of diameter on life time quenching and fluorescence signal enhancement. They showed quenching of the fluorescence lifetime increases with smaller waveguides, likely due to the more efficient energy transfer between fluorophore and metal when they are closer together. Quenching increases radiative rate which increases the emission signal, but the maximum signal is not found at the smallest waveguide smaller waveguides (see figure 3.2). Instead, Wenger et al. foud it at 120 nm wide waveguides. That same year, Gérard et al. [26] added their findings on similar measurements on fluorescence enhancement performed in aluminium waveguides (see figure 3.3). The change in material has shifted the optimum diameter from 120 nm to 170 nm. No matter what size the waveguide is, gold will enhance the fluorescence more strongly than aluminium. Since aluminium will be the choice of metal in this research, the waveguides thus need to be around 170 nm big in order to observe optimal enhancement. To allow for optimization experiments for specific combinations of samples and fluorophores, waveguides of various diameters ranging from 100 to 200 nm were fabricated.

[1]This is the largest diameter of a circular waveguide made out of a perfect metal such that the resulting wavefront is evanescent.

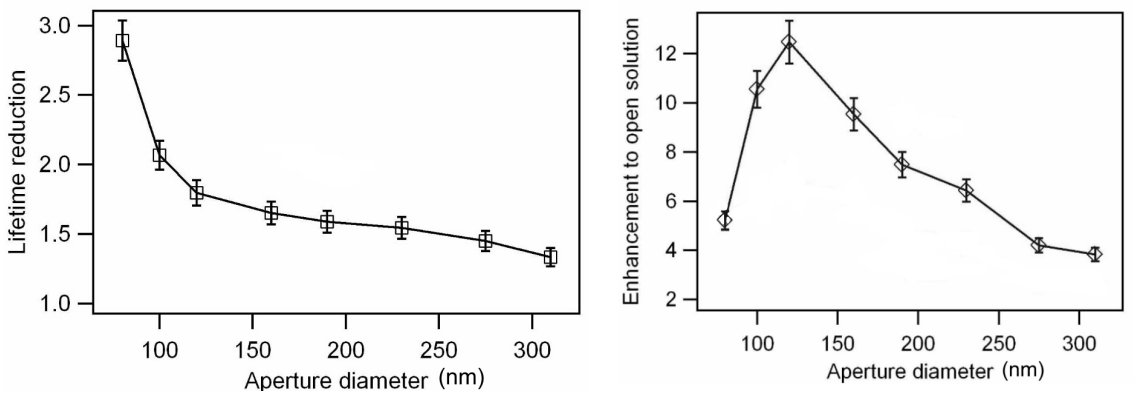

Figure 3.2: Lifetime reduction and fluorescence enhancement in waveguides in 200 nm thick gold, measured with AF647 excited at 633 nm. Adapted from [25].

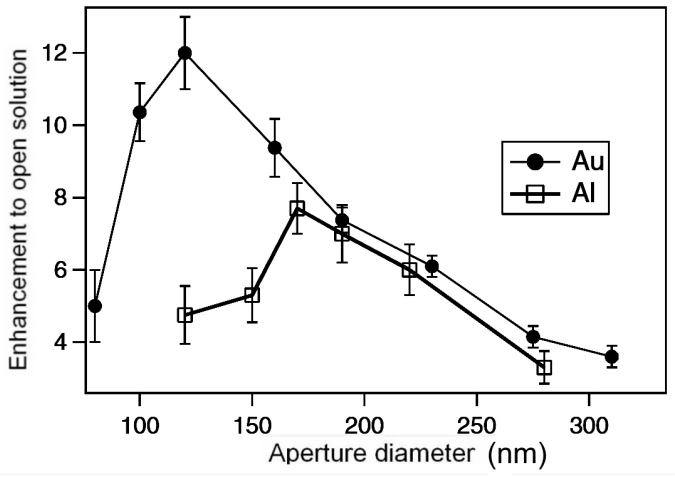

Figure 3.3: Fluorescence enhancement in waveguides in 200 nm thick aluminium, measured with AF647 excited at 633 nm. Adapted from [26].

A final thing to keep in mind when performing measurements using multiple dyes (when investigating FRET for instance) is that the excitation wavelength varies during the experiments which will also affect the fields in the waveguide. Baibakov et al. [22] are one of many to include numerical simulations of the ZMWs in their work (see figure 3.4) which shows the difference in field strength between excitation wavelengths. A careful look will reveal that the enhanced field corresponding to the lower excitation wavelength will penetrate slightly further (or decreases slightly slower) into the waveguide, implying that also the detection volume will be slightly larger. They took this matter into account by spatially averaging the data over the detection volume. Since no numerical simulations have been performed in this study, this remains to be just a thought to keep in mind.

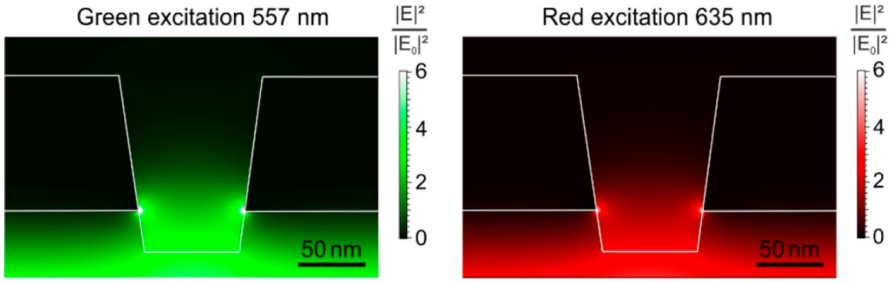

Figure 3.4: Numerical simulations of the excitation field in different size ZMWs using 557 nm and 635 nm excitation wavelengths. Taken from [22].

3.2 Fabrication techniques

Now that the metal and the waveguide size have been determined, fabrication will be the next topic of interest. There are a seemingly endless amount of ways to create nanostructures, but only few of them seem popular amongst other researchers (see table 3.2). The technique most often used is milling using a focussed ion beam (FIB). Another technique used by multiple authors is lithography (using either colloids, CL, or an electron beam, EBL). During lithography [29], a template of sorts is used to pattern a surface, after which a film - in this case aluminium - is deposited on the template. The excess metal as well as the template are then removed.

Focussed ion beam milling	Colloidal lithography	Electron beam lithography
Wenger 2008 [25]	Prikulis 2004 [30]	Foquet 2003 [23]
Nüesch 2022 [16]	Fisher 1981 [31]	Levene 2003 [17]
Patra 2020 [21]	Li 2017 [8]	
Popov 2005 [32]	Krewer 2017 [33]	
Rigneault 2005 [24]		
Gérard 2008 [26]		

Table 3.2: Overview of the three most used fabrication methods reported in consulted literature.

Each fabrication technique has its own advantages and disadvantages, as explained by Gu et al. [34]. The FIB used for milling has very high lateral resolution compared to lithography methods (that either rely on light or colloids), which means the control of the structures is better with a FIB. Additionally, the fabrication is instant, i.e. no need for curing or lifting off excess material. However, Gu et al. remarked that the ions from the FIB could contaminate the surface, although no mentioning of this issue has come across in other work. In cases where one would need many waveguides at once, CL is an interesting technique because it allows for the creation of many waveguides at the same time. However, the whole process in general is more complicated and time consuming. For example, the CL process from Hanarp et al. [35] requires multilayer precursors with rinsing and drying between applying every layer, adding the colloids (PS balls, in this case) and finally a last step to prevent aggregation of the colloids before curing. This will yield merely the template, actually depositing the metal and removing the balls again calls for a different process all together. However, once completed, a collection of holes of homogeneous size can be expected. How large the holes are depends on the size of the colloids, which is a limiting factor in this technique. Additionally, the distance between the holes is more or less random. With a FIB, both the size as well as spacing can be precisely controlled. This is illustrated in figure 3.5. Due to the precise control and flexibility of waveguide size required for optimization experiments, FIB milling was the fabrication technique selected for this ZMW performance study.

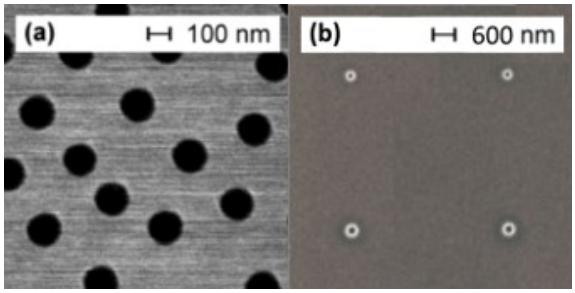

Figure 3.5: (a): taken from [30]. Nanoapertures fabricated with colloidal lithography: irregular pattern, heterogeneous hole size. (b): Taken from [7]. Nanoapertures made by FIB milling: regular pattern and precise diameter control.

During the actual fabrication process, glass coverslips (Marienfeld No. 1.5H) of 170 μm thick and with an area of 22x22 mm^2 were used as substrates. 150 nm aluminium was sputtered on the glass (see section A.1 for details), after which it was placed under a FIB (Thermo Scientific Helios 5 UX Dualbeam, MESA+) for milling. Each coverslip had 5 ZMWs in it, one slip had holes ranging from 100 to 140 nm, the other slip had holes between 150 and 200 nm. All holes were milled 200 nm deep. A schematic of the cross section of the holes can be found in figure 3.6. Around each set of holes, markers were put in place to find the waveguides using a confocal microscope. Additionally, it allows for identification of the individual holes. Figure 3.7 shows a schematic of the design and the confocal image recorded using a mircoscope. Figure 3.8 shows an SEM image of the same coverslip.

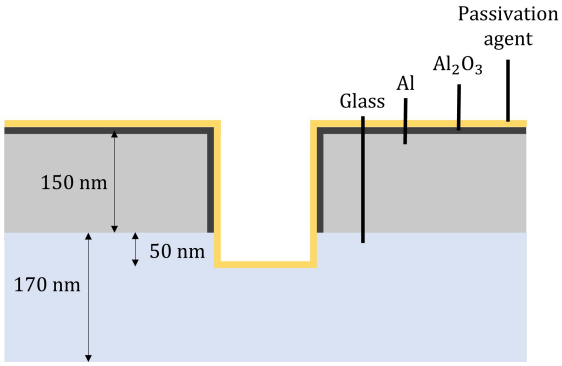

Figure 3.6: Schematic of the cross section of the waveguide in the coverslip after fabrication

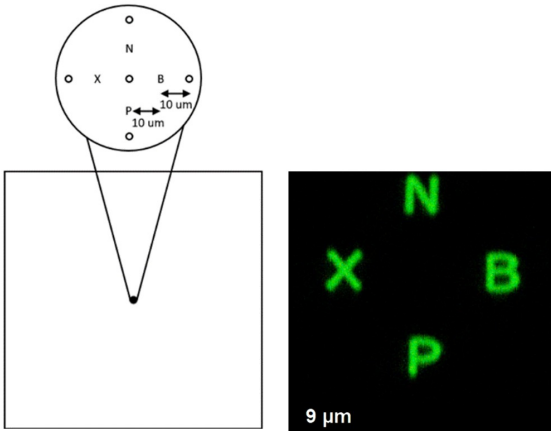

Figure 3.7: Schematic representation of the design of the waveguides in the coverslip and the corresponding confocal microscopy image under the microscope

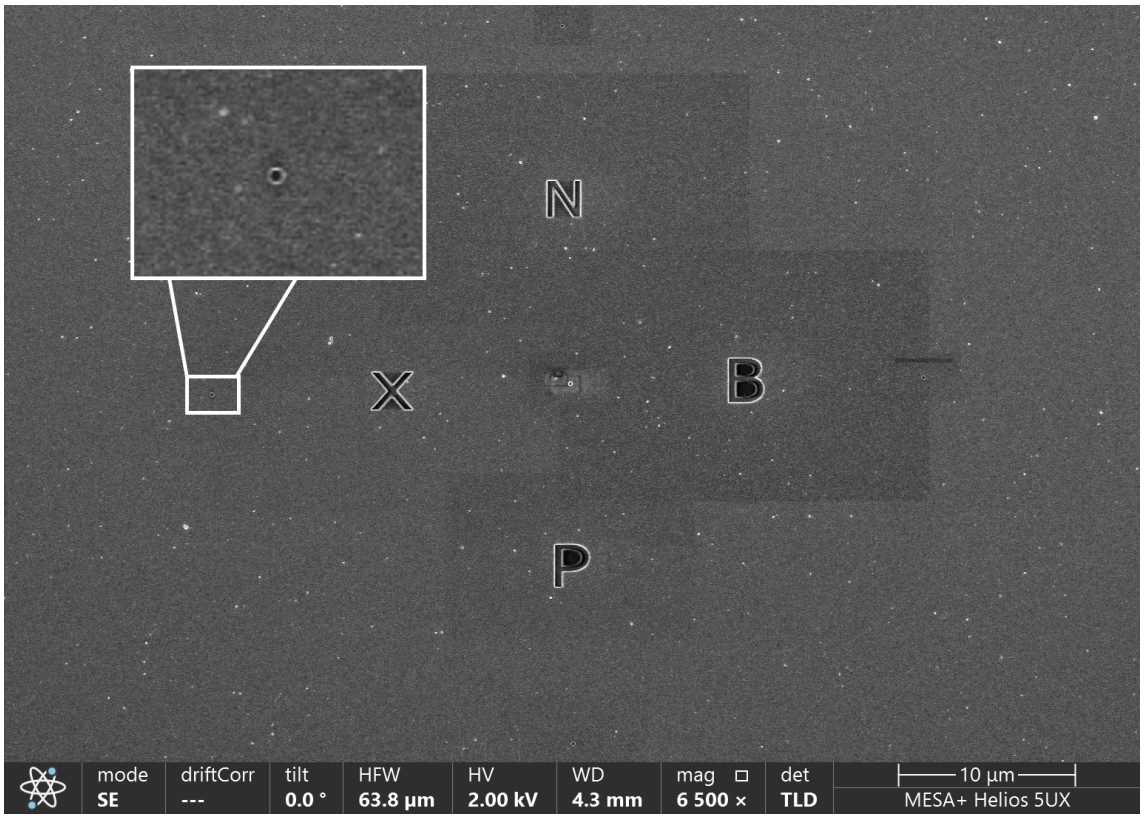

Figure 3.8: SEM image of one of the coverslips. The inset shows one of the ZMWs.

3.3 Validation experiments

In order to asses the performance of the prototype ZMWs and the effectiveness of the various (unconventional) passivation agents, two experiments with basic samples were devised. First, the behaviour of just a dye (Atto 647 N, or A647N) in the ZMW was compared to open solution using two different passivation agents. Then, an aSyn molecule was labelled with a single dye (AF594) and studied in much the same way using unlabelled aSyn as passivation agent. The results will be discussed in the following sections.

3.3.1 A647N

A647N has been dissolved in milliQ (87 nM) and used as a sample in i) open solution, ii) an unpassivated ZMW, iii) a ZMW passivated with BSA and lastly iv) a ZMW passivated with Alexa Fluor 488. The ZMW used had a diameter of 180 nm. According to Patra et al. [21], A647N is expected to adsorb to the aluminium affecting the amount of molecules in the detection volume as well as the diffusion time. They also remarked that BSA was not an effective passivation agent. Testing these two conclusions forms a good starting point for this research. Since no PEG was available at the time, an alternative passivation protocol was improvised using Alexa Fluor 488 molecules. Although not shown in this work, AF488 also seemed to adsorb heavily. This is expected to prevent A647N from adsorbing, making AF488 a suitable passivation agent. Additionally the emission of AF488 and A647N can be separated easily which means the emission from AF488 will not interfer with the measurements.

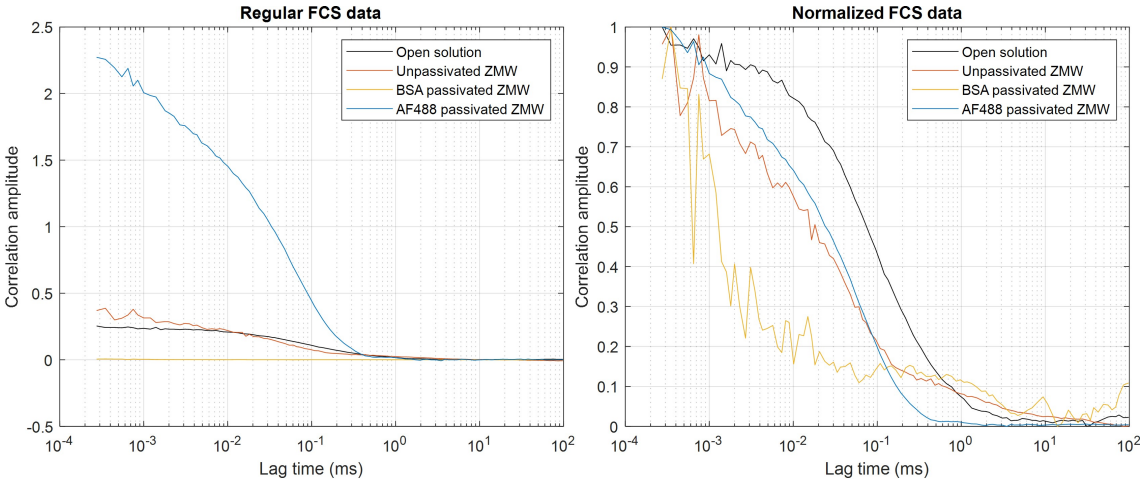

Figure 3.9: FCS data obtained from passivation experiments using 87 nM A647N dye inside ZMW passivated with two different passivation agents. A measurement in open solution is included for reference.

To evaluate the adsorption of A647N on each of the samples, 20 second long time trace measurements were performed. The FCS data obtained from these measurements (regular and normalized) are shown in figure 3.9. The unpassivated ZMW and the open solution measurements both show similar maximum amplitudes of around 0.3. The AF488-passivated ZMW measurement shows a maximum amplitude almost an order of magnitude higher (up to 2.3) and the BSA-passivated measurement shows barely an amplitude at all at this scale, compared to the open solution measurement. Since the correlation amplitude is inversely proportional to the average number of molecules in the detection volume, this means that there are much more molecules present in the BSA-passivated ZMW than expected. The unpassivated ZMW holds a similar number of molecules as the open solution measurements, but it is expected to house less: given the concentrations are the same, the smaller detection volume inside the ZMW should decrease the occupancy. This implies that the molecules adsorb to and/or interact with the surface, causing a higher average

molecule count.

The normalized FCS data gives more insight in the behavior of the molecules. Since the detection volume is smaller, the A647N molecules are expected to reside in them less long: the diffusion time is expected to decrease, thus the width at half maximum (WHM) should decrease compared to open solution. All three measurements performed in the waveguides show this effect. The open solution measurement has the longest diffusion time (around 0.0745 ms), followed by the unpassivated and the 488 passivated ZMW (0.0184 ms and 0.0240 ms, respectively. A decrease of about 75% compared to open solution). The fastest molecules can be found in the BSA-passivated ZMW, with a (unreasonably quick) diffusion time of 0.0013 ms. Also note the difference in shape of the BSA-passivated measurements compared to the three others: it does not seem to converge to a single value at lower lag times. These two facts indicate this system is behaving very differently and in a unpredicted way: for this reason, as well as the conclusion of Patra about its effectiveness as a passivation agent, it was decided to exclude BSA from future experiments.

There is a second region of interest in these curves apart from the WHM: the tail-end. The slower a molecule, the more correlation exists for higher lag times: the presence of an additional component alludes to adsorption effects within the waveguide. The transition to this 'adsorption component' is especially noticeable in the case of the unpassivated ZMW (note the kink in the normalized FCS data at a lag time of 0.15 ms). It does not show up in the AF488-passivated ZMW measurement, but it is present in the other two cases. This likly means no adsorption takes place when the ZMW is passivated with AF488, where it would occur if left unpassivated or is passivated with the wrong agent.

Now that a suitable passivation agent has been identified, the other parameters related to the use of ZMWs can be investigated: lifetime quenching and fluorescence enhancement. In order to find the fluorophore lifetime, TCSPC data is collected and shown in figure 3.10. The ZMW measurement decays faster than the measurement taken in open solution, indicating shorter lifetime. The PicoQuant software can then fit a numerical (exponential) model, allowing for extraction of the lifetime components[2]. For the open solution, it found a lifetime of 3.53 ± 0.0034 ns, whereas the measurement in the ZMW provided a lifetime of 1.93 ± 0.0089 ns. The lifetime of the A647N dyes in the ZMW was about 1.8 times smaller than the lifetime measured in open solution, proving that the fabricated ZMWs indeed quench fluorophore lifetime.

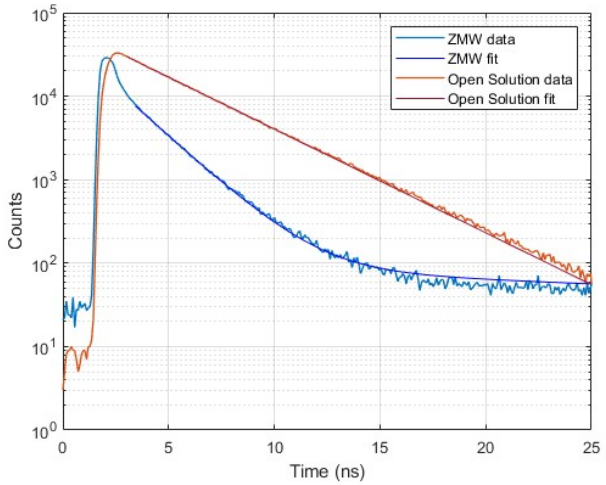

Figure 3.10: TCSPC data obtained from open solution and ZMW measurements using A647N dye.

[2]In the waveguides, a two component model could be fitted. The reported lifetime corresponds to intensity averaged lifetime, corresponding to the mean arrival time of a photon.

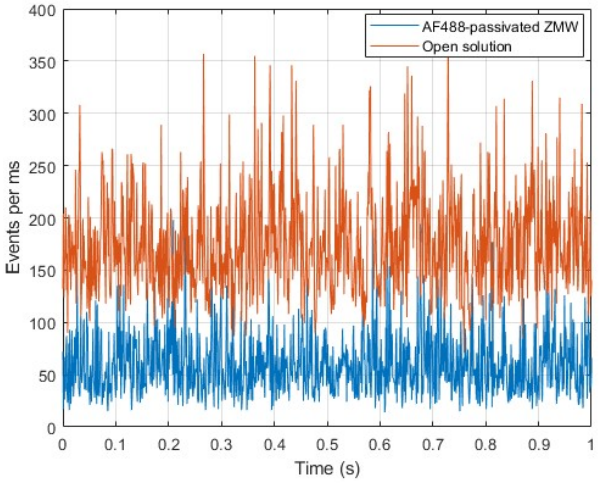

Figure 3.11: Time trace data obtained from open solution and ZMW measurements using A647N dye. In both cases, the sample concentration was 87nM.

Lastly, the time traces with AF488 passivation as well as the measurement in open solution can be found in figure 3.11. Both were measured with 87nM A647N. At first glance, it seems the ZMW has not increased but decreased the signal, as the time trace clearly shows less events in the ZMW measurement compared to the open solution measurement ($CR_{OS} \approx 170$ events per ms for open solution and $CR_{ZMW} \approx 60$ events per ms for the ZMW). This is because the amount of molecules in the detection volume has not been taken into account: there are more molecules in open solution, so the signal they collectively produce is higher. To compare the two, the average number of molecules is obtained from the FCS data in figure 3.9, which results in $< N_{OS} > \approx 1/0.25 \approx 4$ for open solution and $< N_{ZMW} > \approx 1/2.3 \approx 0.4$ for the AF488 passivated ZMW. Combined with the CR, this yields a CRM of approximately 40 for open solution and a CRM of about 150 for the ZMW. Clearly, the signal per molecule is more than three times higher in the ZMW compared to open solution which proves the capability of the waveguides to enhance fluorescence signal.

3.3.2 aSyn AF594

Next, fluorophores were actually used to label a protein as would be the case in regular TCCD or FCS experiments. In this case, aSyn was labelled with AF594. Past experiences in the group led to believe aSyn is a particularly sticky molecule, in the sense that it adsorbs strongly to glass and possibly metal. Where previously the fluorophore was found to adsorb it was assumed that here, the sample molecule rather than the dye would cause adsorption problems. In order to prevent aSyn from adsorbing during the measurements, the ZMW was coated with a solution of 5 μM unlabelled (wild type) aSyn: the idea being the aSyn-WT would saturate the surface leaving no possibility for labelled aSyn to adsorb. To test this, another experiment was divised: a solution of 100 nM aSyn-AF594 was measured using passivated and unpassivated ZMWs and data was collected immediately after depositing the sample, 10 minutes after depositing and finally 20 minutes after depositing. The longer the sample was left to sit, the more molecules would adsorb, and the larger the FCS amplitude must become[3]. The FCS curves corresponding to this experiment are shown in figure 3.12.

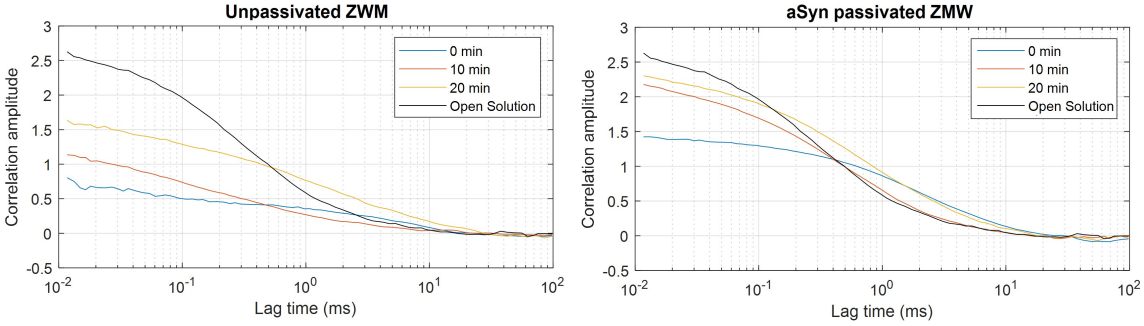

Figure 3.12: FCS curves of aSyn-AF594 measurements on an unpassivated ZMW and a ZMW passivated with aSyn-WT for different time. Open solution measurements at 100 pM have been included for reference.

The data shows that in both cases, the FCS amplitude increases with increasing time of measurement, which means the average number of molecules in the detection volume decreases. However, between the passivated and unpassivated ZMW, there exists a key difference: the degree to which the amplitude increases between the different measurement times is almost constant in the case of an unpassivated ZMW. This implies a continuous loss of sample molecules due to adsorption. In the case of the aSyn-WT passivated ZMW we see a strong increase of amplitude followed by only a relatively small one, which suggests the loss of molecules slows down and almost stops after 10 minutes. Figure 3.13 shows the amount of molecules in the detection volume over time. The fact that not only less molecules reside in the detection volume of the passivated ZMW for the same concentration, but also that the change in rate at which this number decreases is different, suggests that adding aSyn-WT does prevent some aSyn-AF594 molecules from adsorbing, but not all. However, that does not explain why the diffusion time between 10 and 20 minutes on the passivated ZMW increases by a little more than 1.5 times (0.43 ms for 10 minutes versus 0.67 ms for 20 minutes). No explanation for this has yet been found.

[3]At the same time, solvent wil evaporate at a certain rate. This rate is assumed to be smaller than the rate of adsorbtion. The change in $< N >$ is a net result of the two.

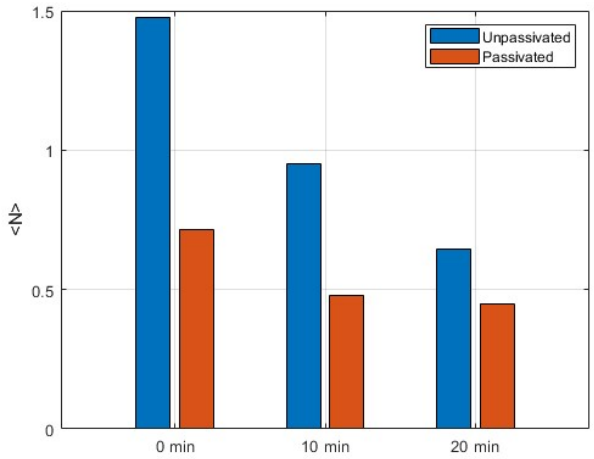

Figure 3.13: Average number of molecules in the detection volume, obtained from the data in figure 3.12 for a passivated and unpassivated ZMW.

As interesting a sidestep as this is, the more relevant conclusion is the fact that aSyn-WT proves not to be a suitable passivation agent for aSyn-AF594 measurements, as all FCS curves show some higher lag time component. The time trace data shown in figure 3.14 tells the same story, evident from the broad peaks at for instance 0.2 s and 0.8 s in the passivated ZMW: clearly molecules 'stick around' longer in the volume than expected. Also note that, despite the adsorption, the signal is still increased. The CRM in open solution is 53, the CRM in the ZMW is 101. However, since the time trace measured in the ZMW has broader peaks the number of counts is higher for longer, which increases the average more than a properly passivated ZMW would. This should be kept in mind when comparing these data sets.

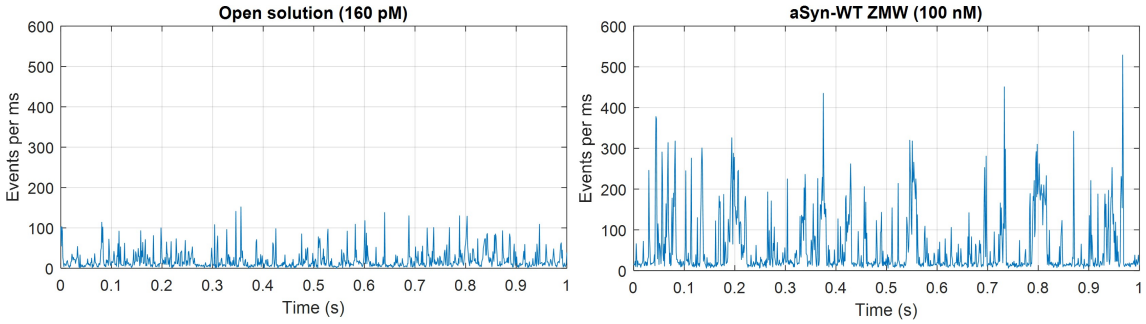

Figure 3.14: Time trace data for aSyn-AF594 sample in open solution and in a ZMW passivated with aSyn-WT. The ZMW data corresponds to that collected after 20 minutes.

All in all, the validation experiments have shown that the ZMWs that have been manufactured do indeed work in the sense that lifetime is quenched, fluorescence signal is enhanced and that burst traces can be obtained using moderately high ($1\ nM \leq C \leq 1\ \mu$M) concentrations. They also show that proper surface passivation can be achieved in some cases, but there is no underlying theory or method to base it on: no reliable or general solution - like PEG or PVPA promised to be - has been found. The next chapter will move on from these conceptual experiments and discus the more interesting experiments related to biomolecular interactions in ZMWs.

Chapter 4

Probing biomolecular interactions in zero-mode waveguides

This chapter will show the experiments related to molecular interactions. Both aSyn as well as DNA have been used to perform or simulate such reactions. The primary goal of this chapter is to show that i) burst traces can be obtained in ZMWs at concentrations exceeding the picomolar range and that ii) adsorption of sample to the surfaces of the waveguides can be prevented using a proper passivation agent. Additionally, this chapter will show how such a burst measurement - in the case of DNA - can lead to insight in molecular reactions using a TCCD experiment. TCCD will also be used as a means to estimate whether the ZMW affects the samples at all. The association quotient as determined in an open solution measurement should be the same as one determined inside the ZMW, which will be investigated for both the aSyn and DNA sample.

4.1 aSyn AF568-AF647

First, aSyn was double labelled with AF568 (donor) and AF647 (acceptor) and mixed together in a 1:1 ratio. Ultimately, being able to measure interactions between aSyn and 14-3-3 is of interest. However, the behaviour of 14-3-3 in the ZMW has not been investigated yet, so for now double labelled aSyn will be used. This section will first show how proper surface passivation has been obtained after which it will show the burst traces obtained and quantify the fluorescence enhancement.

Passivation using aSyn-WT

In a first effort to establish surface passivation, ZMWs were passivated using unlabelled aSyn (aSyn-WT) using the protocol described in section 2.2. Although multiple validation experiments have shown that aSyn-WT is not a suitable passivation agent, nothing else was at hand at the time. The double labelled aSyn sample was measured at 3 different concentrations (1 μM, 100 nM, 10 nM). The three different concentrations were a sidestep to see the effect of sample concentration on the behaviour of the sample molecules, much like the way in which aSyn-AF594 was measured at various time intervals to see the effect of the passivation. To assess the performance of aSyn-WT as a passivation agent, the 100 nM double labelled aSyn sample was also measured inside a unpassivated ZMW. The normalized FCS data obtained from these experiments is shown in figure 4.1. From the FCS data the diffusion constant can be obtained and like before the correlation at lag times $\tau \geq 10$ ms can be used to judge whether or not the molecules show adsorption. Although not included here, a measurement in open solution (100 nM) has also been performed, yielding a diffusion time of 0.5 ms. This value can be used as an upper limit for the diffusion time in the ZMWs.

The FCS data measured in an unpassivated ZMW shows striking behaviour: its shape is fundamentally different from any other reported so far. With a diffusion time of over 30 ms and a large peak in correlation at a lag time of 500 ms, it is clear adsorption slows down the molecules

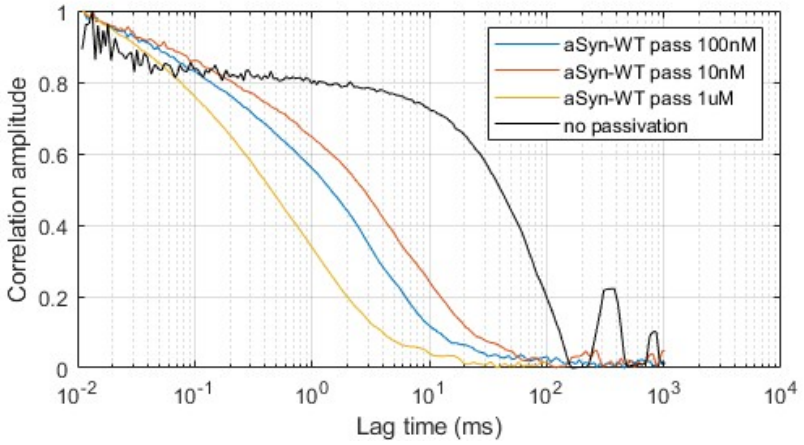

Figure 4.1: FCS data for the double labelled aSyn sample at various concentrations measured in an aSyn-WT passivated ZMW, compared to the same sample measured at 100 nM in an unpassivated ZMW. The data corresponds to the direct acceptor data.

significantly. At first glance, the passivated ZMWs seem to behave as expected. However, as subtle as it is compared to the unpassivated ZMW measurement, there is still an additional correlation component at lag times over 100 ms. This indicates adsorption regardless and its present regardless of the sample concentration. Do note that the larger the sample concentration is, the smaller the effect seems to be. In the 10 nM FCS data (red curve), the transition from regular FCS data to additional component is very clear from the kink at a lag time of 25 ms. In the FCS data collected from the 1 μM sample, there is a transition at a lag time of 60 ms, but it is far more subtle: it could almost be regular fluctuations. This is believed to be due to the fact that the fraction of molecules that has not absorbed to the surface is larger in samples with higher concentrations. This large fraction of 'free molecules' suppresses the adsorption effect in the diffusion time caused by the relatively small fraction of adsorbed molecules, making the transition in the FCS data less noticeable. Based on figure 4.1, it can be concluded that aSyn-WT does reduce passivation, but it does not prevent it completely. This is in line with the earlier conclusion regarding the concept measurement of aSyn-AF594 in section 3.3.2..

This conclusion is also evident in the time traces shown in figure 4.2. In both the unpassivated waveguide as well as the aSyn-WT passivated one, broad peaks show up. However, the peaks are on average less broad when the sample is measured in the aSyn-WT passivated ZMW. Additionally - on occasion - proper intensity bursts with a width smaller than approximately 0.10 ms are visible (for example at 0.1 and 0.2 seconds in the direct acceptor time trace) in the passivated waveguides. It is clear that in these ZMWs, molecules remain less long in the detection volume and move in and out more, given that there are far more peaks per second. Because the broad peaks and the actual bursts have comparable magnitude, the adsorption hinders the burst analysis. All in all this means that aSyn-WT is indeed not a suitable passivation agent for aSyn AF568-AF647 measurements. Therefore, a different passivation agent must be found. Rather than improvising with the samples at hand, silane modified PEG was purchased and used to passivate the waveguides: similar to what Nüesch [16] and Patra [21] have done.

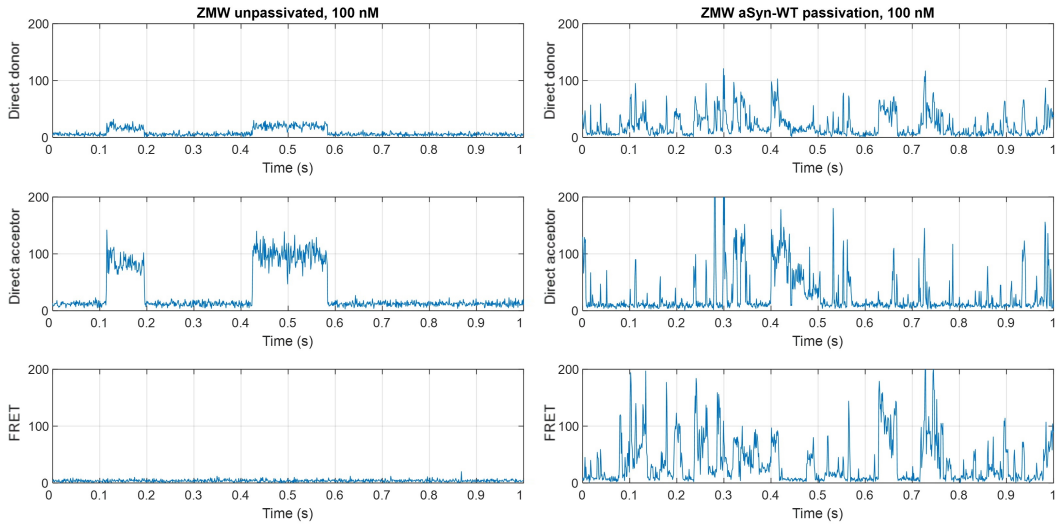

Figure 4.2: Time traces (events per ms) for an unpassivated ZMW and a ZMW passivated with aSyn-WT. In both cases, 100 nM of double labelled aSyn was measured.

Passivation using silane-PEG

The passivation protocol described in section 2.2 has been used to passivate the waveguides with silane-modified PEG with a weight of 1000 Da. The same double labelled aSyn sample described before was measured at 100 nM on these waveguides, and for reference the same sample at 100 pM was measured in open solution. Figure 4.3 shows the time traces obtained from these experiments. Once the ZWMs were passivated with PEG, the broad absorption peaks observed with aSyn-WT passivation almost disappeared, indicating that almost no aSyn sample adsorbs to the surface. Occasionally, a broader peak like the ones in figure 4.1 was found, but its event rate was comparable to the noise level which made it easy to discriminate between proper bursts and adsorption. Unfortunately, the SNR for direct donor and FRET has decreased significantly compared to open solution. This makes it harder - but not impossible - to discriminate bursts from noise. For direct acceptor emission, the signal to noise level has increased by a vast amount. The CRM in the ZMW for the direct donor emission is found to be 1.5k and that of the acceptor 4.0k. In open solution, the donor has a CRM of 34 compared to 16 for the acceptor: the ZMW has enhanced the signal 44 times for the donor and 250 times for the acceptor, although it must be noted that the increase in direct donor emission in the ZMW largely consists of higher noise ratios, evident from the time trace.

The total acquisition time of the ZMW measurement was 500 seconds, during which neither the burst rate nor the intensity seemed to decrease, signifying excellent yet uncanny stability (see figure 4.4). Burst analysis can be performed on the time traces in the ZMW and open solution which results in an association constant of 0.23 in open solution versus 0.28 in the ZMW. Since these values are very similar, it can be concluded that the ZMW did not affect the sample. Although PEG passivation seems to work very well, later attempts at measuring this sample have not been successful. Because of that, interaction experiments between aSyn and 14-3-3 were not possible and more experiments must be conducted to perfect the passivation protocol first.

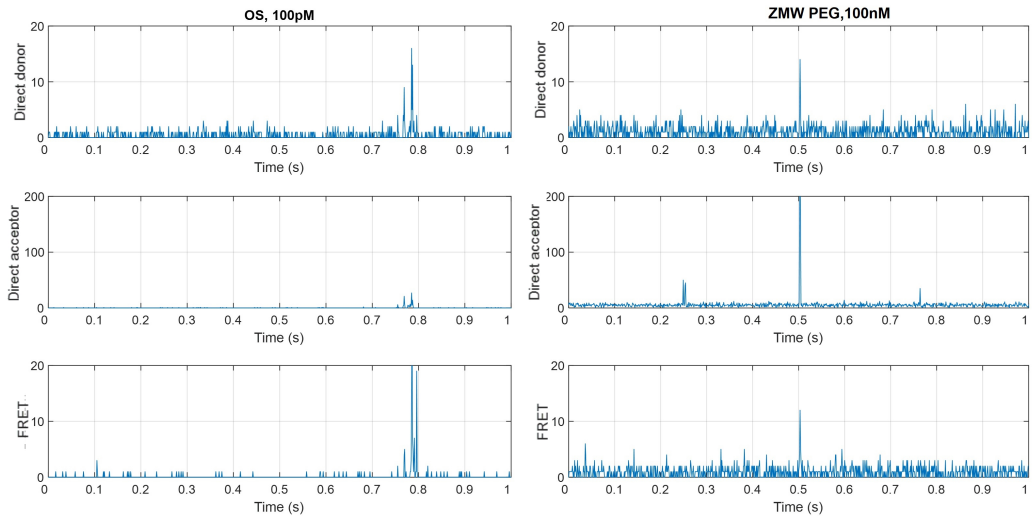

Figure 4.3: Time traces (events per ms) for a double labelled aSyn sample measurement in open solution and in a ZMW passivated with PEG. Note the difference in scale between direct donor and FRET events and the direct acceptor events.

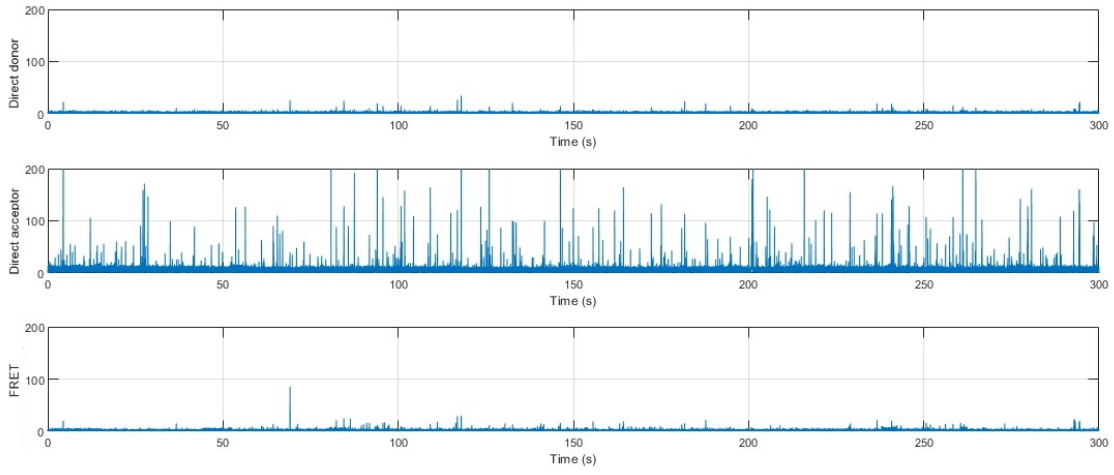

Figure 4.4: Full time traces (events per ms) for the double labelled aSyn sample measured in a ZMW passivated with PEG during a 5 minute experiment. The sample was measured at a concentration of 100 nM.

4.2 DNA A488-A565

Apart from aSyn, DNA molecules have also been investigated in this report. In part, because the passivation protocol for DNA provided more consistent results than that of aSyn, allowing for the opportunity to measure different types of DNA samples. Furthermore, the ability to measure more than one type of molecule on a ZMW would increase the flexibility and the ease of use of the waveguides: there would just be one set of ZMWs for all samples. This section will show the experiments and results of DNA. One DNA strand was labelled with a donor (Atto 488) and its complementary strand was labelled with an acceptor (A565). The two were mixed at a 1:1 ratio and diluted to 100 nM. First, the effectiveness of the passivation with unlabelled DNA will be investigated. Then, the time trace and count rate will be discussed. In order to simulate molecular interaction a TCCD experiment has been devised, where burst traces of two different ratios of complementary DNA strands have been measured. Finally, the TCCD experiment was repeated with one of the samples in waveguides of varying diameter in an attempt to find an optimum diameter for the enhancement of the fluorescence emission.

Adsorption and diffusion time

Figure 4.5 shows the FCS data obtained from acceptor emission after acceptor excitation (direct acceptor emission). Unlike unlabelled aSyn, unlabelled DNA actually seems to prevent adsorption as can be seen from the FCS data shown in figure 4.5 and the time traces in figure 4.7. The FCS curve measured in the unpassivated ZMW (blue) shows a small baseline for lag larger than 1 ms, where the DNA-passivated ZMW does not. Also, the time traces do not show the broader peaks that were present in the aSyn-WT passivated sample. Lastly, the diffusion time of the acceptor in the ZMW is shorter than that in open solution. All of this suggest that indeed no adsorption takes place.

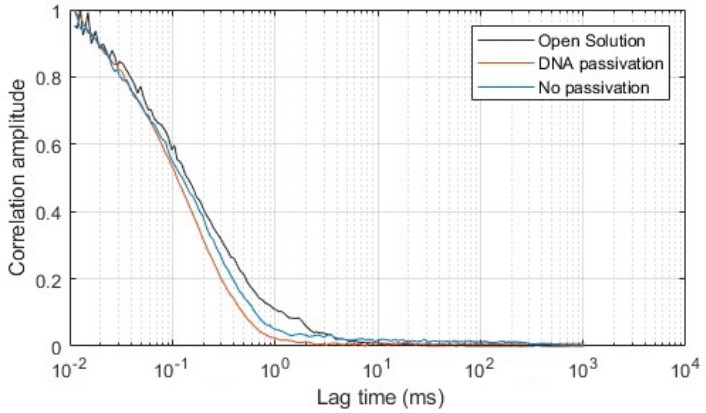

Figure 4.5: FCS data for the double labelled DNA sample (10 nM) in open solution and in a ZMW (100 nM). The data corresponds to the direct acceptor emission.

Using the unlabelled DNA as a passivation agent, the FCS curves corresponding to direct donor and direct acceptor emission in the ZMW can be compared to open solution. These plots are show in figure 4.6. Since the donor and acceptor fluorophores are bound to the same DNA molecule, their diffusion times should be the same (provided the detection volumes are equal in size and ignoring differences in excitation laser powers). However, in both the open solution as well as the ZMW data there exists a difference between the diffusion times, where the difference in the ZMW is more present than in open solution. The difference in diffusion time in open solution between donor and acceptor is about 18%, in the ZMW this difference is approximately 80% (in both cases, the diffusion time of the acceptor is larger than that of the donor). In both open solution as well as in the ZWM, the detection volumes are actually not the same. Since the confocal volume (open solution) is limited by the diffraction limit, the light used for donor excitation (488 nm) creates

a smaller volume than the light for acceptor excitation (560 nm). Therefore, the diffusion time for the donor should be slightly smaller than that of the acceptor, which is indeed the case. In the ZMW, one would expect the detection volume for the donor to be slightly larger since smaller wavelengths penetrate the waveguides slightly further as Zhu and Craighead [27] showed. Thus the diffusion time for the donor should be slightly larger. However, the diffusion time for the donor is smaller. No explanation for this phenomena has yet been found, yet it is believed to be a combination of the difference in laser powers as well as the location of the focal plane in the waveguide.

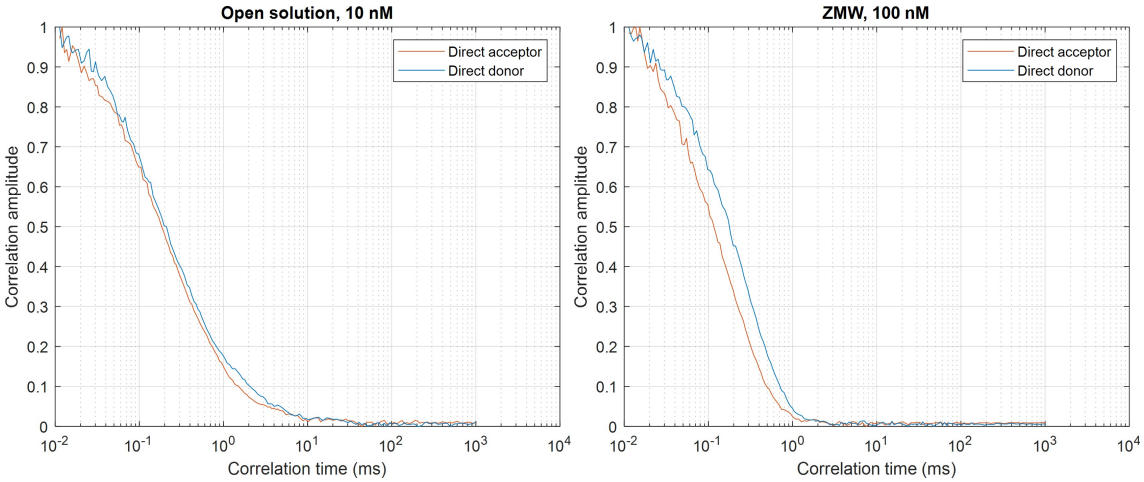

Figure 4.6: FCS data for the double labelled DNA sample in open solution (10 nM) and in a ZMW (100 nM) for both direct donor as well direct acceptor emission.

Time trace and count rate

The time trace data collected in open solution and in the ZMW is shown in figure 4.7. Since the excitation wavelengths are different depending on the type of emission, the degree of enhancement will be different between them. Three important conclusions can be drawn from the data: i) single molecule bursts can be measured with a concentration up to 100 nM, ii) the amount of bursts per unit time (burst rate) in the ZMW is larger than in open solution and iii) the amplitude of the bursts in the ZMW is larger than in open solution. Using the FCS data, the CRM and enhancement can be defined. For direct donor emission, the CRM increases from approximately 2.0 to approximately 5.0. For direct acceptor, the CRM increases from around 9.0 to 52 (open solution and inside the ZMW respectively).

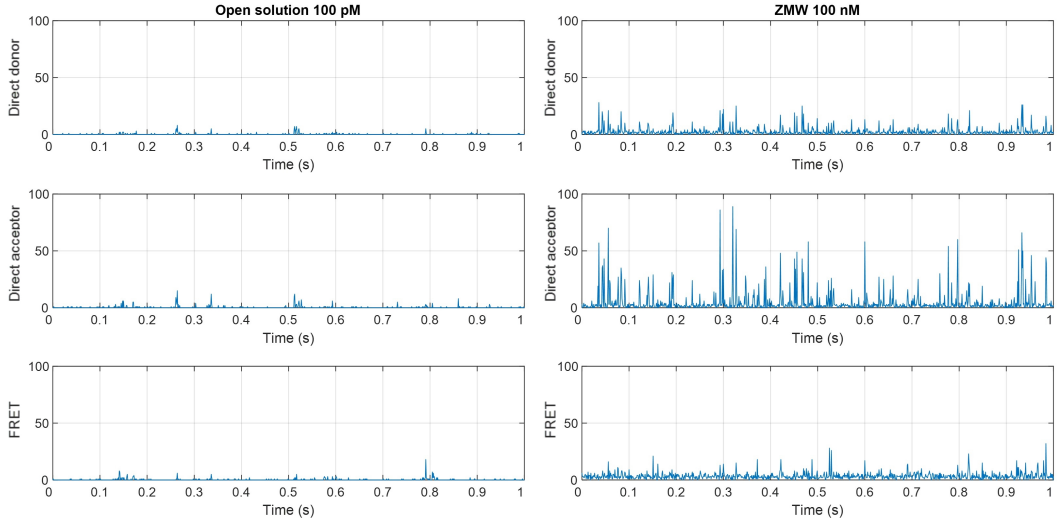

Figure 4.7: Time trace data (events per ms) for the direct donor, direct acceptor and FRET channels. The orginal measurement was 20 seconds long. The ZMW is passivated with unlabelled DNA and has a diameter of 172 nm.

TCCD and association quotient

Using TCCD, the association quotient of a sample can be determined. To perform TCCD experiments a DNA strand labelled with a donor (A488) is combined with its complementary strand labelled with an acceptor (A565). One sample in which these partners are mixed together 1:1 and one where they are mixed at a 3:4 ratio are measured in both open solution and in ZMW, with suitable concentrations to obtain single molecule detection. Of each sample, the time traces are collected for burst analysis. These traces are also shown in figure **??**. This analysis reveals the value of the association constant Q. The samples were measured for 1800 seconds in open solution and 15 sets of 20 second measurements were performed in the ZMWs. Table 4.1 shows the values for Q, the ratio of the number of detected direct acceptor and direct donor bursts and the ratio of the direct donor and direct acceptor CRM for each measured sample.

	Medium (D-label:A-label)	**Q**	$\frac{directacceptorbursts}{directdonorbursts}$	$\frac{CMRdirectacceptor}{CMRdirectdonor}$
1:1 sample	OS (80pM:80pM)	0.18	1.3	1.2
	ZMW (80nM:80nM)	0.19 (std 0.07)	9.2	2.5
3:4 sample	OS (60pM:80pM)	0.16	1.7	1.3
	ZMW (60nM:80nM)	0.19 (std 0.07)	11.2	2.5

Table 4.1: Results of the TCCD experiment with DNA.

The value of Q in the open solution measurement does not differ that much between a 1:1 and a 3:4 mixing ratio: it decreases by approximately 10%. The values for the ZMW however seem statistically equivalent: in both samples, the same average association quotient was found, with the same standard deviation. Although these average values of Q contain their reference value in open solution within the standard deviation, making a hard claim based on just these results is troublesome. In general, the fact that the value of Q between the 1:1 and 3:4 experiment changes so little is remarkable. Two other parameters, the ratio of detected bursts and the ratio between the CRM, also provide an indication of how similar the results between open solution and ZMW are. Between the 1:1 and 3:4 sample in open solution, the ratio of detected bursts increases by 31%: relatively, there are more burst detected in the acceptor channel compared to the donor

channel. This is in line with the decrease of donor labelled DNA going from 1:1 to the 3:4 sample. In the ZMW this increase (22%) is also observed, though the absolute value of the ratios differ: this is elaborated on in the next paragraph. Finally, the ratio of CRM of acceptor labelled DNA and donor labelled DNA remains virtually constant between the 1:1 and the 3:4 sample, regardless of whether it was measured in open solution or the ZMW. This makes sense, as the relative concentration should not affect the count rate per molecule. In light of all of these factors, it may be concluded that the ZMW does not significantly alter the results of a TCCD measurement.

However, this conclusion should be put into context of the difficulties experienced with the burst analysis. Like with the aSyn measurements, the CR and the SNR of the donor compared to that of the acceptor was not great, evident from the ratios between detected donor and acceptor bursts listed in table 4.1. On average, there were 10 times less direct donor bursts with a standard deviation in burst rate twice that of its direct acceptor equivalent, which reduced precision when determining Q. One of the time traces from the 3:4 measurement in the ZMW has been included in figure 4.8A. Figure 4.8B shows how many burst could be obtained from that same time trace. Notice how the number of donor only bursts is much smaller than the number of acceptor bursts, leading to the high burst rate ratio of 11.2. Also note that almost all (approximately 90%) of the detected donor bursts coincide with a (non random) acceptor event. This begs the question why the determined value of Q was so low.

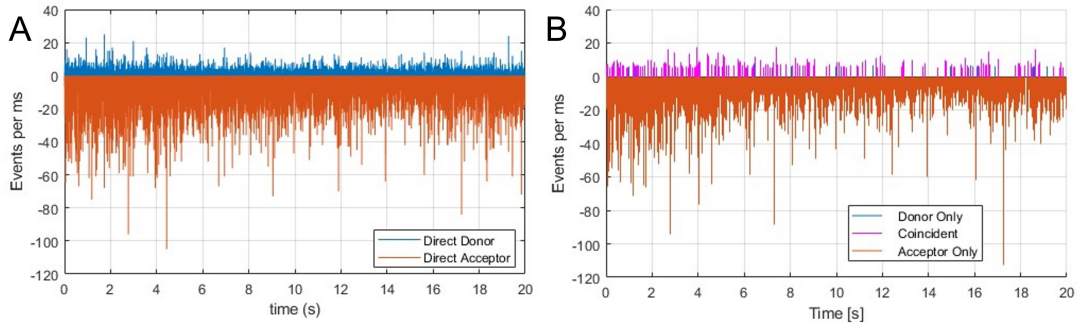

Figure 4.8: A: time trace and B: detected bursts of one of the donor labelled DNA (60 nM) and acceptor labelled (80 nM) TCCD measurement in the ZMW. The magenta peaks correspond to non random coincident bursts between the donor and acceptor channel.

Optimization of waveguide diameter

The experiment with a 1:1 sample can be repeated for differently sized ZMWs. An additional 7 ZMWs with sizes ranging between 100 nm and 200 nm were measured, obtaining fluorescence enhancement, diffusion times and expected number of molecules. The results can be found in figure 4.9.

Starting with the average numbers of molecules in figure 4.9A, for both the direct donor as well as the direct acceptor data this number seems to be larger for smaller holes. Additionally, there are more donor molecules in the detection volume for all waveguides. This could be a consequence of the difference in detection volumes because of the difference in excitation wavelength, but if that were the case such a big discrepancy is expected to also appear in the diffusion time data in figure 4.9B. It does not. Apart from the difference between donor and acceptor being that larger, the trend also does not seem to behave that straightforwardly either. If the waveguide gets smaller, less molecules are expected to reside in it. That was the hole point of introducing them in the first place: being able to get less molecules in the detection volume. However, the data shows a decrease in the amount of molecules with increasing waveguide diameter. This is likely a consequence of the (faulty) way in which the number of molecules is extracted from the data.

Figure 4.9B shows the diffusion time obtained from the FCS data for various waveguide sizes as well as open solution. As previously mentioned before, the diffusion time of the donor is expected

to be slightly larger than that of the acceptor due to the difference in detection volume. This seems to be the case only for the smaller waveguides, and the relative difference between them is not constant either. This may be ascribed to the uncertainty in the values of the diffusion times, since no model was used to fit them: only raw experimental data. However, the general trend does seem to make more sense than that of $< N >$: as the waveguide increases - and with it the detection volume - the diffusion time also increases. It even seems, specifically for the donor - to even tend to the value found in open solution. The diffusion time of the acceptor seems to overshoot that value in the 182 nm waveguide only to slightly decrease back to it in the 192 nm waveguide. Again, this might be due to some experimental error.

Next, the fluorescence enhancement shown in figure 4.9C. As expected, there is an optimum that can be identified. For both the donor and acceptor, the highest recorded fluorescence enhancement can be obtained by using a waveguide of 172 nm wide. A smaller, local maximum can be found at the 115 nm waveguide, but it is so small - and out of place - that it might well be experimental error. The optimum diameter of approximately 170 nm matches the findings of Gérard et al. [26], who also found this optimum (experimentally and numerically) using aluminium waveguides and AF647 dyes. Note that the time traces in figure 4.7 show larger signal for direct acceptor emission in the ZMWs than the direct donor emission, which corresponds to the enhancement in figure 4.9C: clearly the emission of the acceptor is enhanced about twice as strongly as that of the donor.

Finally, the lifetime reduction is shown in figure 4.9D. Both acceptor and donor lifetimes are reduced more strongly for smaller waveguides. The data corresponding to the acceptor seems to follow the trend quite well, the donor data shows quite some variation. The actual amount of reduction is slightly larger than what Gérard reported.

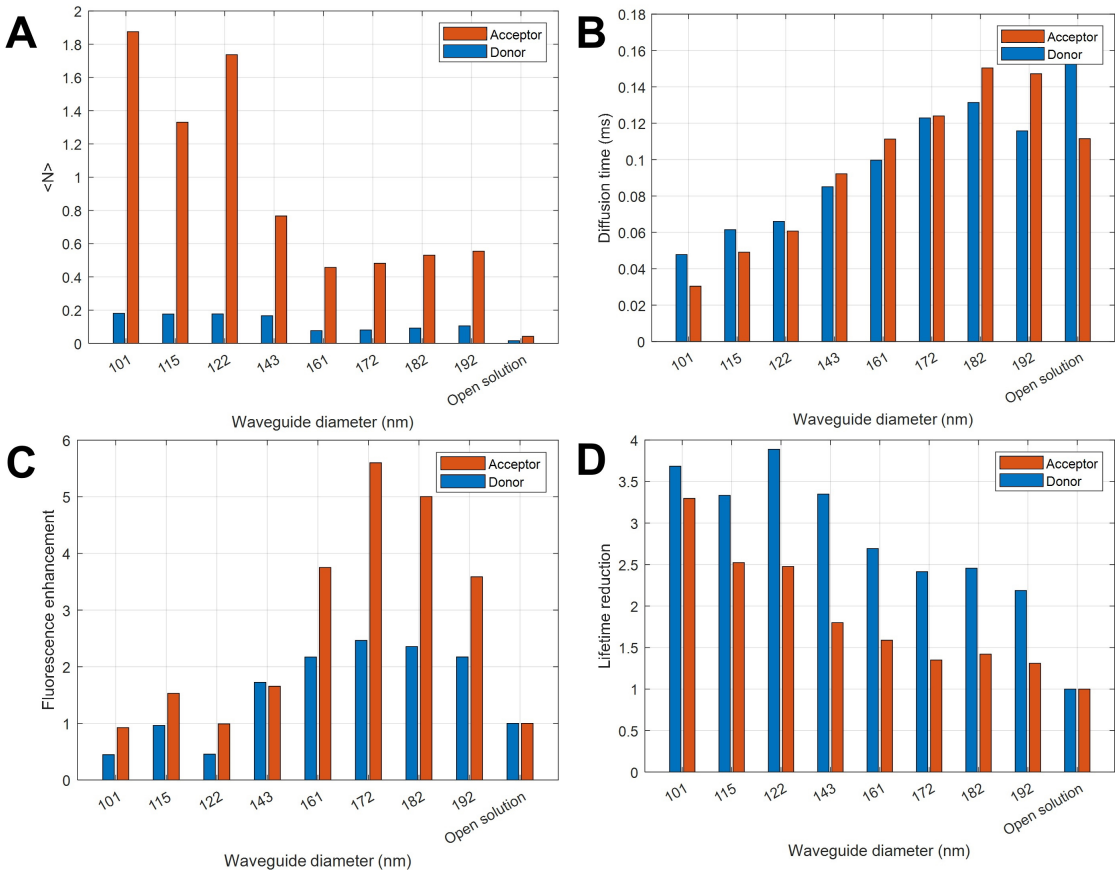

Figure 4.9: Effect of waveguide diameter on A) the average number of molecules in the detection volume, B) the diffusion time of the DNA, C) the fluorescence enhancement for the double labelled DNA sample and D) the lifetime reduction.

Chapter 5

Conclusions and outlook

This report has shown that it is possible to design and create ZMWs in a relatively quick and simple way using FIB milling. The produced prototype ZMWs have been subjected to experiments to evaluate the degree to which they enhance fluorescence signal and quench the lifetime of fluorophores and to perform single molecule detection with higher concentrations than what is accessible in conventional fluorescence methods. A major part of this investigation has consisted of limiting non-specific adsorption to the surface of the ZMW, which in part has been successful. After running experiments with basic samples, an attempt was made to probe biomolecular interactions of aSyn and DNA. Unfortunately, the passivation protocol for aSyn has not yet proved to be consistent, which prevented experiments involving aSyn and 14-3-3. Passivation protocols with DNA did perform to standard, which allowed for TCCD experiments with complementary DNA strands.

There is a number of items that still require further research. Below, the most important ones are listed in arbitrary order.

- Investigation of the depth of the ZMWs should be conducted. Currently, only holes of 200 nm deep and an aluminium layer of 150 nm were used, such that the waveguides would protrude into the glass. Different layer thicknesses might improve the SNR, which turned out to be a challenge in the direct donor data from the DNA and aSyn measurements
- The aluminium for the ZMW has been sputtered on the cover slips. This resulted in a relatively rough film, which made it harder to control the size of the holes during FIB milling. It might also have contributed to adsorption effects. Different deposition techniques, like vapour deposition techniques. It is also worth looking into the claim posed by Baibakov et al. [22] about the importance of aluminium deposition parameters during fabrication and the optical losses they can introduce. In general, more emphasize should be placed on the metal coating process while discussing fabrication.
- The passivation protocol with silane modified PEG for the aSyn measurements needs to be further examined and tested to allow for interaction measurements. Because its effectiveness was found to be so inconsistent, further measurements could not be performed
- To possibility of performing nsFCS measurement inside ZMWs has not yet been investigated using DNA and/or aSyn, although the promise of smaller acquisition times does make it a very interesting possibility
- Data analysis protocol needs to be improved, specifically considering the determination of the amount of molecules in the detection volume. The current assumption that the triplet state can be circumvented by clipping the FCS data between 10^{-2} -10^{2} ms is not a suitable method.
- Although not suitable for experiments with AF488 or A488, gold ZMWs should be investigated too. They have been shown to enhance fluorescence signal even further which might help in increasing the SNR.

Bibliography

[1] Association France Parkinson, "Parkinson's disease: alpha-synuclein, a major factor?," 2018. URL https://www.youtube.com/watch?v=68y-3frzSSY.

[2] C. B. Lücking and A. Brice, "Review Alpha-synuclein and Parkinson's disease," tech. rep., 2000.

[3] F. Emamzadeh, "Alpha-synuclein structure, functions, and interactions," *Journal of Research in Medical Sciences*, vol. 21, no. 1, p. 29, 2016. doi:10.4103/1735-1995.181989.

[4] M. Goedert, "Alpha-synuclein and neurodegenerative diseases,"

[5] M. G. Spillantini, M. L. Schmidt, V. M.-Y. Lee, J. Q. Trojanowski, R. Jakes, and M. Goedert, "α-Synuclein in Lewy bodies," *Nature*, vol. 388, pp. 839–840, 8 1997. doi:10.1038/42166.

[6] R. Gordon, "Metal Nanoapertures and Single Emitters," *Advanced Optical Materials*, vol. 8, 10 2020. doi:10.1002/ADOM.202001110.

[7] D. Punj, P. Ghenuche, S. B. Moparthi, J. de Torres, V. Grigoriev, H. Rigneault, and J. Wenger, "Plasmonic antennas and zero-mode waveguides to enhance single molecule fluorescence detection and fluorescence correlation spectroscopy toward physiological concentrations," 2014.

[8] J. Li, C. Dong, and J. Ren, "Strategies to reduce detection volume of fluorescence correlation spectroscopy (FCS) to realize physiological concentration measurements," 4 2017.

[9] J. Lakowicz, *Principles of Fluorescence Spectroscopy*. Boston, MA: Springer US, 2006. doi:10.1007/978-0-387-46312-4.

[10] J. K. G. Karlsson, A. Laude, M. J. Hall, and A. Harriman, "Photo-isomerization of the Cyanine Dye Alexa-Fluor 647 (AF-647) in the Context of dSTORM Super-Resolution Microscopy," *Chemistry – A European Journal*, vol. 25, pp. 14983–14998, 11 2019. doi:10.1002/chem.201904117.

[11] "Atto-tec," 2022.

[12] N. Mushero and A. Gershenson, "Determining serpin conformational distributions with single molecule fluorescence," in *Methods in Enzymology*, vol. 501, pp. 351–377, Academic Press Inc., 2011. doi:10.1016/B978-0-12-385950-1.00016-X.

[13] A. Orte, R. Clarke, S. Balasubramanian, and D. Klenerman, "Determination of the Fraction and Stoichiometry of Femtomolar Levels of Biomolecular Complexes in an Excess of Monomer Using Single-Molecule, Two-Color Coincidence Detection," *Analytical Chemistry*, vol. 78, pp. 7707–7715, 11 2006. doi:10.1021/ac061122y.

[14] C. M. D'Antoni, M. Fuchs, J. L. Harris, H.-P. Ko, R. E. Meyer, M. E. Nadel, J. D. Randall, J. E. Rooke, and E. A. Nalefski, "Rapid quantitative analysis using a single molecule counting approach," *Analytical Biochemistry*, vol. 352, pp. 97–109, 5 2006. doi:10.1016/j.ab.2006.01.031.

[15] P. Holzmeister, G. P. Acuna, D. Grohmann, and P. Tinnefeld, "Breaking the concentration limit of optical single-molecule detection," *Chem. Soc. Rev*, vol. 43, p. 1014, 2014. doi:10.1039/c3cs60207a. URL http://www.brenda-enzymes.org/.

[16] M. F. Nüesch, M. T. Ivanović, J. B. Claude, D. Nettels, R. B. Best, J. Wenger, and B. Schuler, "Single-molecule Detection of Ultrafast Biomolecular Dynamics with Nanophotonics," *Journal of the American Chemical Society*, vol. 144, pp. 52–56, 1 2022. doi:10.1021/jacs.1c09387.

[17] M. J. Levene, J. Korlach, S. W. Turner, M. Foquet, H. G. Craighead, and W. W. Webb, "Zero-Mode Waveguides for Single-Molecule Analysis at High Concentrations," *Phys. Rev. Lett*, vol. 416, no. 2, p. 2022, 2002. URL `https://www.science.org`.

[18] J. R. Lakowicz, "Radiative decay engineering 5: Metal-enhanced fluorescence and plasmon emission," *Analytical Biochemistry*, vol. 337, pp. 171–194, 2 2005. doi:10.1016/J.AB.2004.11.026. URL `www.elsevier.com/locate/yabio`.

[19] P. F. Lenne, H. Rigneault, D. Marguet, and J. Wenger, "Fluorescence fluctuations analysis in nanoapertures: Physical concepts and biological applications," *Histochemistry and Cell Biology*, vol. 130, pp. 795–805, 11 2008. doi:10.1007/S00418-008-0507-7.

[20] K. Tanaka, M. Tanaka, and T. Sugiyama, "Creation of strongly localized and strongly enhanced optical near-field on metallic probe-tip with surface plasmon polaritons," tech. rep., 2006.

[21] S. Patra, M. Baibakov, J. B. Claude, and J. Wenger, "Surface passivation of zero-mode waveguide nanostructures: benchmarking protocols and fluorescent labels," *Scientific Reports*, vol. 10, 12 2020. doi:10.1038/s41598-020-61856-9.

[22] M. Baibakov, S. Patra, J.-B. Claude, A. Moreau, J. Lumeau, and J. Jero Me Wenger, "Extending Single-Molecule Fo rster Resonance Energy Transfer (FRET) Range beyond 10 Nanometers in Zero-Mode Waveguides Article," *ACS Nano*, vol. 13, 2019. doi:10.1021/acsnano.9b04378. URL `www.acsnano.org`.

[23] M. Foquet, K. T. Samiee, X. Kong, B. P. Chauduri, P. M. Lundquist, S. W. Turner, J. Freudenthal, and D. B. Roitman, "Improved fabrication of zero-mode waveguides for single-molecule detection," *J. Appl. Phys*, vol. 103, p. 34301, 2008. doi:10.1063/1.2831366. URL `https://doi.org/10.1063/1.2831366`.

[24] H. Rigneault, J. Capoulade, J. Dintinger, J. Wenger, N. Bonod, E. Popov, T. W. Ebbesen, and P.-F. Lenne, "Enhancement of Single-Molecule Fluorescence Detection in Subwavelength Apertures," 2005. doi:10.1103/PhysRevLett.95.117401.

[25] J. Wenger, D. Gérard, J. Dintinger, O. Mahboub, N. Bonod, E. Popov, T. W. Ebbesen, and H. Rigneault, "Emission and excitation contributions to enhanced single molecule fluorescence by gold nanometric apertures," *Optics Express*, vol. 16, no. 5, p. 3008, 2008. doi:10.1364/oe.16.003008.

[26] D. Gérard, J. Wenger, N. Bonod, E. Popov, H. Rigneault, F. Mahdavi, S. Blair, J. Dintinger, and T. W. Ebbesen, "Nanoaperture-enhanced fluorescence: Towards higher detection rates with plasmonic metals," 2008. doi:10.1103/PhysRevB.77.045413.

[27] P. Zhu and H. G. Craighead, "Zero-Mode Waveguides for Single-Molecule Analysis," 2012. doi:10.1146/annurev-biophys-050511-102338. URL `www.annualreviews.org`.

[28] M. Fabian, E. Lewis, T. Newe, and S. Lochmann, "Optical fibre cavity for ring-down experiments with low coupling losses," *Measurement Science and Technology*, vol. 21, 7 2010. doi:10.1088/0957-0233/21/9/094034.

[29] D. Ji, T. Li, and H. Fuchs, "Nanosphere Lithography for Sub-10-nm Nanogap Electrodes," *Advanced Electronic Materials*, vol. 3, 1 2017. doi:10.1002/AELM.201600348.

[30] J. Prikulis, P. Hanarp, L. Olofsson, D. Sutherland, and M. Ka, "Optical Spectroscopy of Nanometric Holes in Thin Gold Films," vol. 19, p. 16, 2004. doi:10.1021/nl0497171. URL `https://pubs.acs.org/sharingguidelines`.

[31] U. C. Fischer and H. P. Zingsheim, "Submicroscopic pattern replication with visible light," *Journal of Vacuum Science and Technology*, vol. 19, p. 881, 1981. doi:10.1116/1.571227. URL https://doi.org/10.1116/1.571227.

[32] E. Popov, H. Rigneault, J. Wenger, J. Dintinger, P.-F. Lenne, and T. W. Ebbesen, "Single molecule fluorescence in rectangular nano-apertures," *Optics Express, Vol. 13, Issue 18, pp. 7035-7044*, vol. 13, pp. 7035–7044, 9 2005. doi:10.1364/OPEX.13.007035. URL https://opg.optica.org/viewmedia.cfm?uri=oe-13-18-7035&seq=0&html=truehttps://opg.optica.org/abstract.cfm?uri=oe-13-18-7035https://opg.optica.org/oe/abstract.cfm?uri=oe-13-18-7035.

[33] K. L. Krewer, K. Jiang, and K. Bley, "Large area conductive nanoaperturearrays with strong optical resonances andspectrally flat terahertz transmission," *Appl. Phys. Lett*, vol. 111, p. 21107, 2017. doi:10.1063/1.4992131. URL http://dx.doi.org/10.1063/1.4992131].

[34] P. Gu, W. Zhang, G. Zhang, P. Gu, W. Zhang, and G. Zhang, "Plasmonic Nanogaps: From Fabrications to Optical Applications," 2018. doi:10.1002/admi.201800648. URL www.advancedsciencenews.com.

[35] P. Hanarp, D. S. Sutherland, J. Gold, and B. Kasemo, "Control of nanoparticle film structure for colloidal lithography," tech. rep.

Appendix

A.1 Sputter parameters

The aluminium was sputtered on the coverslips using the MESA+ Sputterke. The following settings were used:

- 60 second pre-sputter to clean targets before deposition on the cover slips
- Deposition rate of 12 nm/min for 800 seconds at 200 W
- No adhesion layer

A.2 CUTE plasma system settings

Femto Science CUTE plasma system in the PBM lab (ZH227) at the Univeristy of Twente was used to plasma clean the aluminium coates coverslips with the waveguides. Samples were loaded into the chamber. The pressure is reduced to 0.5 *torr* after which the chamber is rinsed with oxygen. Finally, the plamsa is activated at 50 W and the sample is left to clean for 5 minutes. The chamber vents and the sample is removed.

A.3 Optical systems

In combination with the PicoQuant MT200, the following optical systems were used.

	A647N	
	Channel 1	**Channel 2**
Excitation wavelength(s)	640, 10 μW	-
Dichroic mirror	488-640 (Chroma ZT470-488/640rpc-UF3)	-
Optical filters	690/70	-

	aSyn-AF594	
	Channel 1	**Channel 2**
Excitation wavelength(s)	560, 40 μW	-
Dichroic mirror	485-560 (Chroma ZT488/561rpc-UF3)	-
Optical filters	620/60	-

	aSyn AF568-AF647	
	Channel 1	**Channel 2**
Excitation wavelength(s)	560, 14 μW	640, 14 μW
Dichroic mirror	405-485 + 560-638 (Semrock Di03-R405/488/561/635-t3-25x36)	
Optical filters	640 notch 640 LP 690/70	640 notch 620/60

	DNA	
	Channel 1	**Channel 2**
Excitation wavelength(s)	488, 5 μW	560, 5 μW
Dichroic mirror	485-560 (Chroma ZT488/561rpc-UF3)	
Optical filters	560 notch 560 LP 620/60	560 notch 520/35

Table 1: Optical filters and other settings used for the various experiments.